# TRIAXIAL COMPRESSION EXPERIMENTS ON PLAIN CONCRETE

by

Omar G. Flores Pérez

A report submitted in partial fulfillment of the requirements for the degree of

MASTER OF ENGINEERING
in
CIVIL ENGINEERING

UNIVERSITY OF PUERTO RICO
MAYAGÜEZ CAMPUS
December 2009

Approved by:

| | |
|---|---|
| _____ | _____ |
| Miguel A. Pando, Ph.D.<br>President, Graduate Committee | Date |
| _____ | _____ |
| Felipe J. Acosta Costa, Ph.D.<br>Member, Graduate Committee | Date |
| _____ | _____ |
| Ricardo R. López Rodríguez, Ph.D.<br>Member, Graduate Committee | Date |
| _____ | _____ |
| Raúl E. Macchiavelli, Ph.D.<br>Representative of Graduate Studies | Date |
| _____ | _____ |
| Ismael Pagán Trinidad, M.S.C.E.<br>Chairperson of the Department of Civil Engineering and Surveying | Date |

# ABSTRACT

This M.E. project report describes the main aspects and findings of an experimental research project on triaxial compression of plain concrete. The main focus of the research is to study the behavior of plain concrete under increasing axial compression while maintaining different levels of constant lateral confinement. Twenty-two mechanical property tests – four unconfined compression tests, and 18 triaxial compression tests – were completed. The triaxial compression tests exhibited a continuous increase in ultimate compressive stress and strain at failure with increasing confining stress. An empirical failure envelope based on a linear correlation of the compressive strength experimental data obtained through this research is presented. Experimentally determined full stress-strain curves are also presented from standard triaxial tests. These curves are used to determine mechanical properties of the plain concrete such as initial Poisson's ratio and initial tangential modulus, and to provide empirical evidence of the effect that lateral confinement will have on these properties. All findings were compared to previously published data or empirical models and in general were found to be in good agreement.

# RESUMEN

Este informe de proyecto describe los aspectos y hallazgos principales de una investigación sobre compresión triaxial en hormigón no reforzado. El foco principal de esta investigación es estudiar el comportamiento de hormigón no reforzado al ser sometido a un aumento en compresión axial bajo diferentes niveles de confinamiento lateral constante. La motivación para esta investigación es ayudar a evaluar la interacción del núcleo de hormigón en tubos de polímero fibro-reforzado rellenos de hormigón. Se llevaron a cabo veintidós ensayos para determinar propiedades mecánicas – cuatro pruebas de carga axial no confinada y dieciocho pruebas de carga triaxial. Las pruebas de carga triaxial mostraron un aumento continuo en la capacidad de carga axial última y la deformación al momento de falla al aumentar el esfuerzo de confinamiento. Se propone una envolvente de falla determinada experimentalmente basada en una correlación lineal de los datos de compresión axial máxima. A su vez, se presentan las curvas de esfuerzo-deformación obtenidas de las pruebas de carga triaxial llevadas a cabo. Estas curvas se utilizaron para determinar propiedades mecánicas del hormigón no reforzado tales como la razón de Poisson y módulo tangencial inicial para proveer evidencia empírica del efecto que aumentar el confinamiento lateral tiene sobre estas propiedades. Los hallazgos se compararon con datos o modelos empíricos publicados previamente. Las hallazgos se compararon con datos previamente publicados o modelos empíricos y en general las tendencias son similares y concuerdan.

# DEDICATORIA

Este trabajo es dedicado a mi madre Awilda, a mi hermana Pamela y a mi padre Rey.

# ACKNOWLEDGEMENTS

First, I would like to thank God. I would like to thank Dr. Miguel A. Pando, president of my graduate committee for all his support and guidance. I also wish to thank Drs. Felipe J. Acosta, Ricardo R. López, and Raúl E. Macchiavelli, members of my graduate committee for their time, comments, and suggestions.

Special thanks go to my family, friends, and co-workers for their constant support and encouragement.

# TABLE OF CONTENTS

# LIST OF TABLES

# LIST OF FIGURES

# NOTATION

| | | |
|---|---|---|
| a | = | Constant in expression to determine major principal stress at failure |
| ACI | = | American Concrete Institute |
| b | = | Constant in expression to determine major principal stress at failure |
| c | = | Apparent intergranular cohesion |
| d | = | Constant in expression to determine major principal stress at failure |
| D | = | Diameter |
| E | = | Young's modulus |
| $E_0^{tan}$ | = | Initial tangential modulus |
| $f'_c$ | = | Unconfined compressive strength of concrete |
| $f_o$ | = | Peak strength of confined concrete |
| FRP | = | Fiber Reinforced Polymer |
| FHWA | = | Federal Highway Administration |
| g | = | Constant in expression to determine major principal stress at failure |
| h | = | Constant in expression to determine major principal stress at failure |
| H | = | Height |
| $K_1$ | = | Arbitrary constant in expression to determine major principal stress |
| $K_2$ | = | Arbitrary constant in expression to determine major principal stress |
| $K_3$ | = | Arbitrary constant in expression to determine major principal stress at failure |
| $K_4$ | = | Arbitrary constant in expression to determine major principal stress at failure |
| m | = | Constant in expression to determine major principal stress at failure |
| M.E. | = | Master of Engineering |

| | | |
|---|---|---|
| PCC | = | Portland Cement Concrete |
| t | = | Time in days |
| $\varepsilon_{axial\text{-}ult}$ | = | Axial strain at failure |
| $\varepsilon_{hoop\text{-}yield}$ | = | Hoop strain at yield stress |
| $\sigma_1$ | = | Major principal stress |
| $\sigma_{1max}$ | = | Major principal stress at failure |
| $\sigma_{1max\text{-}ave}$ | = | Average major principal stress at failure |
| $\sigma_3$ | = | Minor principal stress |
| $\tau$ | = | Shear stress |
| $\upsilon$’ | = | Instantaneous Poisson’s ratio |
| $\upsilon_i$ | = | Initial Poisson’s ratio |
| $\varphi$ | = | Angle of internal friction |

# CHAPTER 1: INTRODUCTION

This M.E. project report describes the main aspects and findings of an experimental research project on triaxial compression of plain concrete. The main focus of the research is to study the behavior of plain concrete under increasing axial compression while maintaining constant lateral confining stress. Although the topic has been studied to some extent, there is limited experimental data to allow reliable predictions using analytical models.

## 1.1 JUSTIFICATION

For a long time it has been recognized that lateral confinement increases the strength and ductility of plain un-reinforced concrete (Considere 1906, Richart et al. 1928, Gardner 1969, Hobbs 1971). Thus, confinement of concrete has been an important design consideration for structural elements such as concrete-filled steel tubes or even concrete columns with steel stirrups which provide partial confinement. For concrete-filled steel tubes, the confinement provided to the concrete by the outer steel tube, when the member is loaded axially, is considered to be practically constant due to the stress-strain characteristics of steel which quickly reaches yielding at low axial strain levels (Mamlouk and Zaniewski 1999). For the case of a concrete column with steel stirrups, the confinement stresses generated by the stirrups are more complex and are considered to be only partial since the stirrups are typically placed with a longitudinal spacing along the column length. Regardless of type of confinement, constant or partial, its inclusion in design is important since it improves strength and ductility of the structural element.

A relatively recent structural element type composed of concrete-filled FRP tubes or existing concrete columns retrofitted with FRP jackets, have become quite popular. For this more recent application, the external FRP tube or jacket provides variable confinement

stresses which increase linearly as the axial strain of the column increases. This linear variation of the concrete confinement stress is related to the almost linear elastic stress-strain behavior of FRP materials coupled with a brittle failure ($\varepsilon_{hoop\text{-}failure} \approx 0.01$ through 0.02)that typically does not exhibit yielding (Fam 2000). In contrast, as mentioned earlier, confining stresses generated by a steel tube are constant since they reach a yield stress at a relatively early stage of the loading process ($\varepsilon_{hoop\text{-}yield} \approx 0.0035$ through 0.005). Any loading beyond this point of yielding will result in constant confining stresses.

Research on confined concrete has been carried out for project specific concrete mixtures and typically with the main objective of evaluating the ultimate strength of the confined concrete and the axial stress-strain behavior. Review of the relevant literature in the subject indicates that existing studies did not typically focus on studying the volume expansion characteristics, or more specifically the influence of confining stress level (Imran and Pantazopoulou 1996). Furthermore, the few available studies (e.g., Gardner 1969, Fam 2000) consider a simple approach of a linear variation of the Poisson's ratio of the concrete as a function of confinement stress level. This research focuses on the study of the behavior of confined concrete under several confinement levels with special consideration of the volumetric characteristics of the concrete as a function of confining level and strain level. The concrete design is project specific as it is related to an ongoing study of the durability of concrete-filled FRP tubes. However, the contribution is still present given the experimental design which involves detailed monitoring of expansion with axial strain level.

## 1.2 OBJECTIVES

The main objective of this research is to determine the stress-strain behavior and associated volumetric response of plain concrete specimens subjected to triaxial compression under a wide range of confining stresses. More specific objectives include:

- Design a comprehensive experimental program to investigate the stress-strain behavior and associated volumetric response of plain concrete specimens subjected to triaxial compression.
- Determine material parameters such as cohesion intercept, angle of internal friction, initial tangential modulus, and initial Poisson's ratio, among others.
- Develop a high quality set of test data which will allow carrying out a statistical analysis of the test results to evaluate variability of results, generate regression and/or correlations if appropriate.
- Prepare a comprehensive summary report documenting the research project including literature review, experimental design and setup, results, findings, and conclusions.

## 1.3 REPORT ORGANIZATION

Besides this chapter this document is organized in 5 additional chapters. Chapter 2 presents a review of the most relevant literature associated with the subject of confined concrete. The literature was divided in experimental studies and analytical models. Chapter 3 presents a description of the experimental program including a detailed description of the test methodology and the specimen preparation. Chapter 4 presents the experimental results and data analysis obtained from the experimental program carried out for this research project.

Chapter 5 presents a brief comparison of the experimental test results with the results obtained through empirical and analytical formulations. Chapter 6 presents a summary of the results, conclusions, and recommendations of this research project.

# CHAPTER 2: LITERATURE REVIEW

This chapter presents a summary of the most relevant literature found on the general subject of stress-strain behavior of axially loaded confined plain concrete. The chapter presents the literature divided in 2 groups: i) experimental studies, and ii) analytical models.

## 2.1 EXPERIMENTAL RESEARCH

The behavior of concrete under triaxial loading has been studied to some extent. Table 2-1 lists some of the most relevant references regarding experimental studies on triaxial compression of plain (unreinforced) concrete samples. All of these studies agree that an increase in ductility and strength is to be expected when a concrete specimen is subjected to triaxial compression. Furthermore, experimental results indicate that the ultimate stress and corresponding ultimate strain increase with increasing levels of confinement.

Experimental research has shifted its main focus throughout the years. Review of the references listed in Table 2-1 shows that early research examined primarily the effect that confinement would have on the mechanical properties of axially loaded concrete. The early studies focused primarily on the impact of confinement on the ultimate strength, probably due to the limitations on obtaining reliable measurements of axial strain. Early studies resulted in simple theories of failure where an analytical expression for the determination of the peak strength of concrete was formulated and verified with the available experimental data.

More modern research incorporated newer instrumentation and data acquisition methods which allowed more precise measurements of load and deformation during axial compression testing.

Some of the studies listed in Table 2-1 propose empirical models developed from the gathered experimental data. The majority of studies focused on the concrete strength as a function of confinement. Very few studies provide details of stress-strain data or volumetric strain variations during these experimental studies. The volumetric strain as a function of axial strain levels is important for concrete filled FRP tubes since the confinement stress will vary with radial strain levels.

As noted in Table 2-1, available studies have important differences related to sample shape and size, concrete unconfined compressive strength, and range of confining pressures used.

**Table 2-1: Summary of Experimental Research on Triaxial Compression of Plain Concrete**

| Reference | Type of Study | Test information | Main Findings |
|---|---|---|---|
| Considere (1906) | Triaxial compression tests on cement or mortar cylinders | • $f'_c$ = 757, 1057, 1311, 2424 psi<br>• 11.8" D X 31.5" H<br>• $\sigma_3$ = 0, 284, 711, 1422, 2133 psi | • The ductility of mortar and concrete is about 20 times as much when crushed in water under pressure as when in their natural state.<br>• $\sigma_1 = a\,(f'_c) + 4.8\,\sigma_3$<br>• a = 1.0 when $\sigma_3$ = 0 psi and increases linearly to 1.5 when $\sigma_3 \geq$ 600 psi. |
| Richart et al. (1928) | Triaxial compression tests on concrete cylinders | • $f'_c$ = 1050, 2575, 3660 psi<br>• 3" D X 6" H<br>• $\sigma_3$ = 250, 500, 750, 1000, 1500, 2000, 3000, 4000 psi | • Effect of lateral pressure on maximum load<br>• Load-Deformation curves<br>• Inconclusive on correctness of Mohr's Theory applied to failure of concrete in triaxial compression<br>• $\sigma_1 = 4.1 \times f'_c + \sigma_3$ |
| Gardner (1969) | Triaxial compression tests on concrete cylinders | • $f'_c$ = 4000 psi<br>• 3" D X 6" H<br>• $\sigma_3$ = 0, 1250, 2500, 3750 psi<br>• $\nu'$ = instantaneous Poisson's ratio<br>• $K_1$, $K_2$, $K_3$, $K_4$ = arbitrary constants calculated as defined in the article. | • Application of Rowe's theory ("Stress-Dilatancy Relation for Static Equilibrium of an Assembly of Particles in Contact") to the behavior of triaxially loaded concrete.<br>• Improvement of all mechanical properties of concrete under triaxial loading.<br>• For low stresses: $\sigma_1/\nu' = K_1\sigma_3 + K_2$<br>• At failure: $\sigma_{1max} = K_3\sigma_3 + K_4$ |
| Hobbs (1971) | Triaxial compression tests on concrete cylinders | • $f'_c$ = 6482 psi (average)<br>• 2.2" D X 4.3 - 6" H<br>• $\sigma_3$ = 0, 363, 725, 1450, 2176, 2900, 3626 psi | • Increment of compressive strength and strain at failure and the amount of non-linearity prior to failure with increasing confining pressure.<br>• Change of specimen's mode of failure between low and high confining pressures.<br>• At failure:<br>$\sigma_1 = a - (b/t) + (g \log t + h)\sigma_3^{\,d}$<br>or: $\sigma_1 = f'_c + [m - g \log (a - f'_c)]\,\sigma_3^{\,d}$<br>• For the particular concrete tested: a = 46.6, b = 108.4, g = 0.85, h = 5.41, d = 0.863, and 7 days $\leq t \leq$ 56 days or: $f'_c$ in N/mm$^2$, m = 3.68, and $31.2 \leq f'_c \leq 44.7$ N/mm$^2$ |

Notes: $\sigma_1$, $\sigma_3$ = major and minor principal stresses, respectively; $f'_c$ = unconfined compressive strength of concrete; D and H = specimen diameter and height, respectively; $f_o$ = peak strength of confined concrete;

**Table 2-1: Summary of Experimental Research on Triaxial Compression of Plain Concrete (continued)**

| Reference | Type of Study | Test information | Main Findings |
|---|---|---|---|
| Imran and Pantazopoulou (1996) | Triaxial compression tests on concrete cylinders | • $f'_c$ =3075, 6309, 9384 psi<br>• 2.125" D X 4.25" H<br>• $\sigma_3$ = (0, 0.05, 0.10, 0.20, 0.40, 0.70, and 1.0)*$f'_c$<br>• Investigates the sensitivity of the mechanical properties of concrete to an array of physical and experimental variables such as porosity of the concrete, moisture content at the time of testing, and the load path used. | • Expansion due to damage is responsible for the stiffness degradation and the softening of resistance that is observed in concrete with increasing deformation levels.<br>• Under increasing lateral confinement, concrete experienced enhancement of strength and apparent ductility. |
| Rutland and Wang (1997) | Triaxial compression tests on concrete cylinders | • $f'_c$ =3075, 6309, 9384 psi<br>• 2" D X 4" H and 2" D X 6" H<br>• $\sigma_3$ = 0, 250, 500, 1000, 2000, 4000, 6000, and 8000 psi<br>• Authors suggest further research of the possible correlations between strain rate and/or confining stress, and mode of failure. | • The angle of the failure plane relative to the direction of the maximum compressive increases with increasing confining pressure but decreases with increasing strain rate. |
| Sfer et al. (2002) | Triaxial compression tests on concrete cylinders | • $f'_c$ = 4351 psi<br>• 6" D X 12" H<br>• $\sigma_3$ = 0, 218, 653, 1305, 4351, 8702 psi experimental studies. | • The increase in confining pressure leads to a change in the mode of failure and an increase in the maximum axial load-carrying capacity.<br>• At zero or low confinement there is a distributed microcracking and several microcracks, and the response exhibits a well-defined peak and subsequent softening.<br>• Responses observed are similar to those observed in previous<br>• At high confinements, relatively large axial and transversal strains were obtained with monotonically increasing loads leading to horizontal plateaus. There is no distributed cracking and failure occurs with the propagation of a few macrocracks.<br>• The authors use an elastoplasticity framework to interpret the experimental results obtained in their tests. |

Notes: $\sigma_1$, $\sigma_3$ = major and minor principal stresses, respectively; $f'_c$ = unconfined compressive strength of concrete; D and H = specimen diameter and height, respectively; $f_o$ = peak strength of confined concrete;

**Table 2-1: Summary of Experimental Research on Triaxial Compression of Plain Concrete (continued)**

| Reference | Type of Study | Test information | Main Findings |
|---|---|---|---|
| Tan and Sun (2006) | Triaxial compression tests on concrete cylinders | • $f_o$ = peak strength of confined concrete<br>• $f'_c$ = 1501, 3945, 7513, 11235 psi<br>• 4" D X 12" H<br>• $\sigma_3$ = 0, 272, 1088, 1813, 2176 psi | • Strength and ductility of concrete under lateral confinement are influenced by the lateral confining stress. The higher the confining stress, the higher the peak stress and peak strain the concrete can achieve.<br>• $f_o = f'_c(-9.338 + 10.338 * \sqrt{1+1.368\frac{\sigma_3}{f'_c}} - 2\frac{\sigma_3}{f'_c})$ |

Notes: $\sigma_1$, $\sigma_3$ = major and minor principal stresses, respectively; $f'_c$ = unconfined compressive strength of concrete; D and H = specimen diameter and height, respectively; $f_o$ = peak strength of confined concrete;

## 2.2 ANALYTICAL MODELS

Analytical models for plain concrete under triaxial compression have been proposed based primarily on experimental data such as the ones published in the studies listed in Table 2-1. The main objective of most available analytical models is to provide a means to predict the axial strength or stress-strain behavior of concrete subjected to axial loading while confined laterally. Table 2-2 lists some of the most relevant references that were found related to development of analytical models. Most models predict only the peak strength of the confined concrete ($f_o$) but some also provide information on peak axial strain ($\varepsilon_{axial\text{-}ult}$).

**Table 2-2: Summary of Analytical Models for Axially Loaded Confined Plain Concrete**

| Reference | Model | Analytical Approach | Observations |
|---|---|---|---|
| Palaniswamy and Shah (1975) | A model of concrete consisting of cylindrical pieces of aggregates in a matrix of cement paste was analyzed by the plane-stress finite element method | Analytical model based on applying "the structural unit" concept to cylindrical triaxial stresses. | The results obtained from the model were compared to those obtained experimentally by the same authors. The model and the concrete showed a ductile - brittle transition as the confining lateral pressures increased. The model failed to predict experimental stress-strain curves. |
| Cedolin et al. (1977) | Triaxial constitutive law and failure criterion for concrete | Analytical expressions relating the bulk and shear moduli to the first two strain invariants to describe deformational behavior of concrete. Failure criterion expressed as a relation between octahedral shear and normal stresses at failure involving the third stress invariant. | Analysis of available experimental data. Unconfined compressive strengths of the experimental data = 1000 - 4840 psi |
| Gerstle (1981) | Octahedral representation of the stress-strain relations for the general triaxial stress state | Addressed the problem that given the three principal stresses how to predict the corresponding principal strains. Formulation introduces the use of the bulk, shear, and coupling moduli obtained through simplifications of the octahedral stress-strain relations. | Corroborates his findings with available experimental data but suggests further testing to explore the generality of the proposed method. |
| Ahmad and Shah (1982) | A method to predict the ascending and descending parts of the stress-strain curve of concrete subjected to triaxial stresses | Analytical equation based on the knowledge of the peak triaxial compressive strength and the corresponding values of three principal strains. A strength criterion is proposed to predict the triaxial compressive strength. The analytical model is based on concepts of incremental nonlinear elasticity. | Model is compared with available experimental data (prior to failure) from concrete filled steel tubes of different thicknesses. |

**Table 2-2: Summary of Analytical Models for Axially Loaded Confined Plain Concrete (continued)**

| Reference | Model | Analytical Approach | Observations |
|---|---|---|---|
| Ahmad et al. (1986) | Orthotropic model to predict the ascending and descending parts of the stress-strain curves of concrete subjected to triaxial compressive stresses | Proposed orthotropic constitutive model depends on the knowledge of the three principal stresses at the maximum strength, which are obtained through the use of a strength criterion. The constitutive model is based on nonlinear elasticity. | Model compared with available experimental data. The model is based on variable material properties in order to reflect damage in the material. |
| Attard and Setunge (1996) | Empirical axial stress-strain model for confined and uniaxially loaded concrete | The model consists on empirical expressions for peak stress, elastic modulus, strain at peak stress, stress and strain at the inflexion point based on uniaxial compressive strength and confinement level. | Model compared with available experimental data. The model was validated against an experimental study evaluating the effect of the type of aggregate used in the mix. The effect of the inclusion of silica fume in the mix was also studied. The model predictions compared well at low confining pressures over a wide range of concrete strengths from 2900 psi to 18850 psi. |
| Imran and Pantazopoulou (2001) | Plasticity based constitutive model of concrete behavior | A generalized constitutive model that combines the framework of nonassociated plasticity with relevant measures of the state of damage due to microcracking in the material structure. | Includes the effects of the water/cement ratio, degree of saturation at testing, load path used in the tests, level of confining pressure, and volumetric expansion. Uses previously published experimental data to calibrate the model. Their findings support that moisture content significantly affects the characteristics of the failure surface for concrete. |
| Ghazi et al. (2002) | Numerical modeling of confined concrete members | 3D total Langrarian finite element model using the Microplane-M4 formulation with second order effects included. | The constitutive laws represented by the Microplane-M4 result in a rise of peak stress under confining pressure which agrees with experimental observations. The peak confined stress obtained with the model is lower than the peak stress obtained from empirical formulae. The post-peak part of the curve approaches a non-zero stress level, the residual stress level of the confined concrete, but at a much earlier strain than the empirical formulae. Addition of a variable set of parameters as functions of concrete strength and confinement level allows a better fit between analytical and experimental results. |

**Table 2-2: Summary of Analytical Models for Axially Loaded Confined Plain Concrete (continued)**

| Reference | Model | Analytical Approach | Observations |
|---|---|---|---|
| Binici (2005) | Confined concrete model to describe the axial and lateral deformation characteristics of concrete under triaxial compression | Model defines the stress-strain relationship in the axial direction with an elastic region followed by a nonlinear curve. The descending region of σ-ε relationship is defined using a constant failure energy criterion. The Leon-Pramono criterion is used to determine the elastic limit, ultimate strength, and residual capacity of the confined concrete specimen. The lateral deformation is described using the model's function. | Model calibrated with available experimental data. Good agreement was observed in terms of ultimate and residual strength as well as with axial and lateral deformation behavior. |
| Montoya et al. (2006) | Development of three constitutive models intended to analyze confined concrete behavior | Authors develop a concrete dilatation model based on available experimental data. Model is based on a simple parabola fitted to the experimental data. The strength enhancement model is based on the Ottosen-type criterion. Authors propose a formulation for the complete stress-strain curves for concrete subjected to triaxial stresses based on mathematical formulations. | Authors compare models with available experimental data. Good agreement was observed between analytical and experimental results. The strength enhancement model is limited to confinement levels up to 100% of the unconfined compressive concrete strength. |
| Oh and Sause (2006) | Empirical axial stress-strain model for confined concrete under uniaxial compression and an empirical transverse deformation model | Model divides the stress-strain curves in three regions: linear elastic, nonlinear ascending, and nonlinear descending. The proposed transverse deformation model requires five different parameters: transverse strain rate, transverse strain, volumetric strain, secant strain ratio, and transverse plastic strain rate. | Authors compare proposed model with experimental data. The proposed axial stress-strain model exhibits greater accuracy than previously published models. The effectiveness of the transverse deformation model as compared to experimental data is not discussed by the author. |
| Papanikolaou and Kappos (2007) | Confinement-sensitive plasticity constitutive model for concrete in triaxial compression | Model incorporates a three-parameter loading surface, uncoupled hardening and softening functions following the accumulation of plastic volumetric strain and a nonlinear Lode-angle dependent plastic potential function. | Model parameters are calibrated using available experimental data. The model captures adequately ultimate strength, deformation capacity, and residual strength of confined concrete. |

# CHAPTER 3: EXPERIMENTAL PROGRAM

This chapter describes the experimental program carried out for this research project. Specifically the chapter describes the test matrix and the methodology used for the experimental program including sample preparation.

## 3.1 TEST MATRIX

The experimental program was designed to evaluate the stress-strain behavior of plain concrete subjected to axial compression and different levels of lateral confinement. The experimental program also involved measuring the volumetric response of the test specimens and determination of a yield surface based on the Mohr-Coulomb failure criteria. A graphical representation of the Mohr-Coulomb failure criteria is given in Figure 3-1 where c is the apparent intergranular cohesion, φ is the angle of internal friction, and $\sigma_1$, $\sigma_3$ are the major and minor principal stresses, respectively.

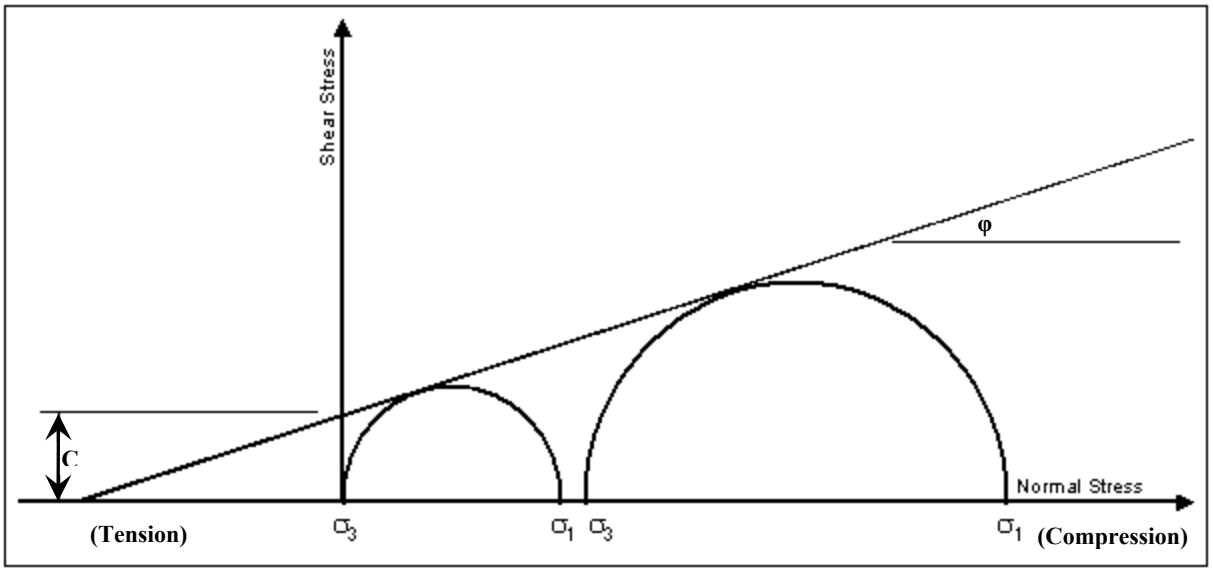


**Figure 3-1: Graphical representation of the Mohr-Coulomb failure criterion**

The experimental program originally involved carrying out 18 triaxial compression tests and 4 unconfined compression tests. Since testing was done during a five month period, it was decided to perform unconfined compressive strength tests prior to every confined compressive strength testing session in order to compare the effect, if any, of additional aging between test series. The final test matrix is summarized in Table 3-1.

**Table 3-1: Test Matrix**

| Confining Stress, $\sigma_3$ (psi) | Number of Triaxial Compression Tests |
|---|---|
| 0 (unconfined) | 4 |
| 500 | 3 |
| 1000 | 3 |
| 1500 | 3 |
| 2000 | 3 |
| 3000 | 3 |
| 4000 | 3 |
| Total number of tests | 22 |

## 3.2 EXPERIMENTAL METHODOLOGY

The following sections describe in detail the concrete mix used in the creation of the cylindrical samples, pre-test sample preparation, instrumentation and test setup, and testing procedures.

### 3.2.1 CONCRETE MIX

The concrete mix used in this research project was the same one used by Dávila (2007) and Lammoglia (in progress) as part of an ongoing research project at UPRM on concrete-filled FRP tubes. This concrete was designed by Dávila (2007) using the PCC-ACI

Absolute Volume Method. The concrete mix was provided by Western Ready Mix Inc. from Mayagüez, Puerto Rico. The cement used was Portland Type I with a maximum coarse aggregate size of 0.375 inches. The 28-day design compressive strength ($f'_c$) was 3000 psi. For this research project only specimens of 2-inch diameter were tested. Dávila (2007) tested larger specimens under unconfined compression.

The curing process for all cylinders involved exposure to ambient humidity during storage. The test samples were stored in a humidity room until testing.

### 3.2.2 COMPRESSION TESTING

All compression tests (unconfined and confined) were carried out at the Structural Laboratory of the University of Puerto Rico at Mayagüez using a MTS 810 Material Test System as shown in Figure 3-2. This load frame is capable of applying a maximum compressive load of 55 kips and allows displacement-controlled testing.

The ends of the concrete cylinders were carefully ground. Figure 3-3 shows the machinery used for this purpose and a close-up on the specimen as it is being ground. This procedure ensured parallel ends that are perpendicular to the longitudinal axis of the cylinder.


**Figure 3-2 MTS 810 Material Test System**

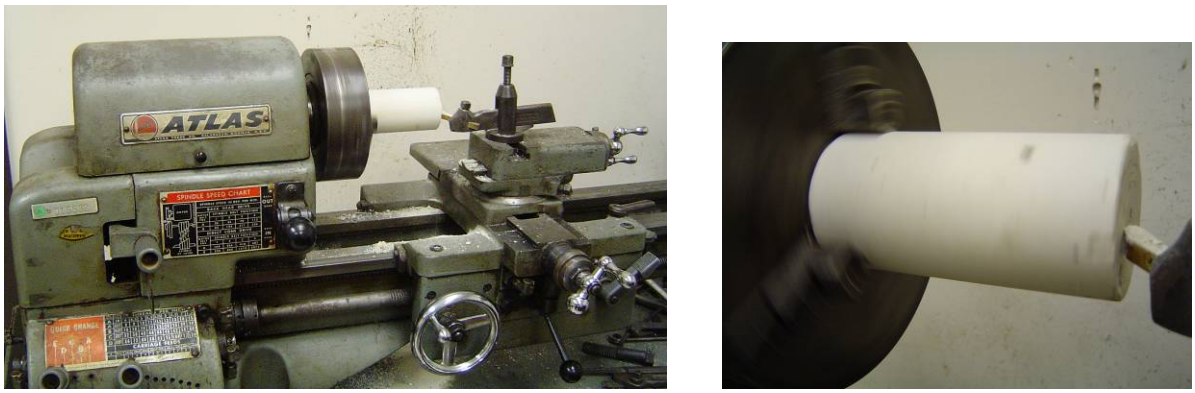


**Figure 3-3: Grinding Machine and close-up on grinding process**

After a specimen was ground to the desired state, it was thoroughly cleaned, identified, measured, and weighed. The next step in the specimen preparation was to identify the longitudinal and hoop at mid-height axes to correctly position the strain gages, two per axis, and each opposing the other as shown schematically in Figure 3-4. The strain gages used were Vishay General Purpose Strain Gages model CEA-06-500UW-350. This strain gages has a resistance of 350 ohms, a gage length of 0.5 inches (12.7 mm), and grid width of 0.18 inches (4.57 mm).

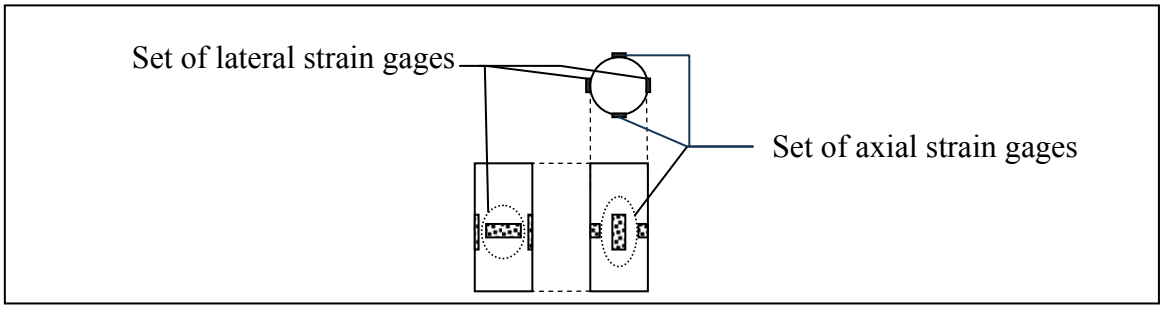


**Figure 3-4: Schematic showing layout of strain gages**

Prior to strain gage installation the surface of the concrete cylinders was prepared in the area where the strain gages were going to be located. The surface area was first lightly sanded to expose any voids that may be covered by the soft superficial concrete. These voids

and any surface irregularities were then filled with DEVCON® 2 Ton® high strength quick set clear epoxy. Once the epoxy was hard it was then sanded and cleaned. This procedure created a smooth surface suitable for strain gage installation. The strain gage installation process is shown in Figure 3-5.

After strain gage installation, the whole surface of the cylinder was inspected for voids that could harm the rubber membrane used in triaxial tests. Therefore for confined triaxial tests surface voids, if any, were filled with the same high strength epoxy described previously.

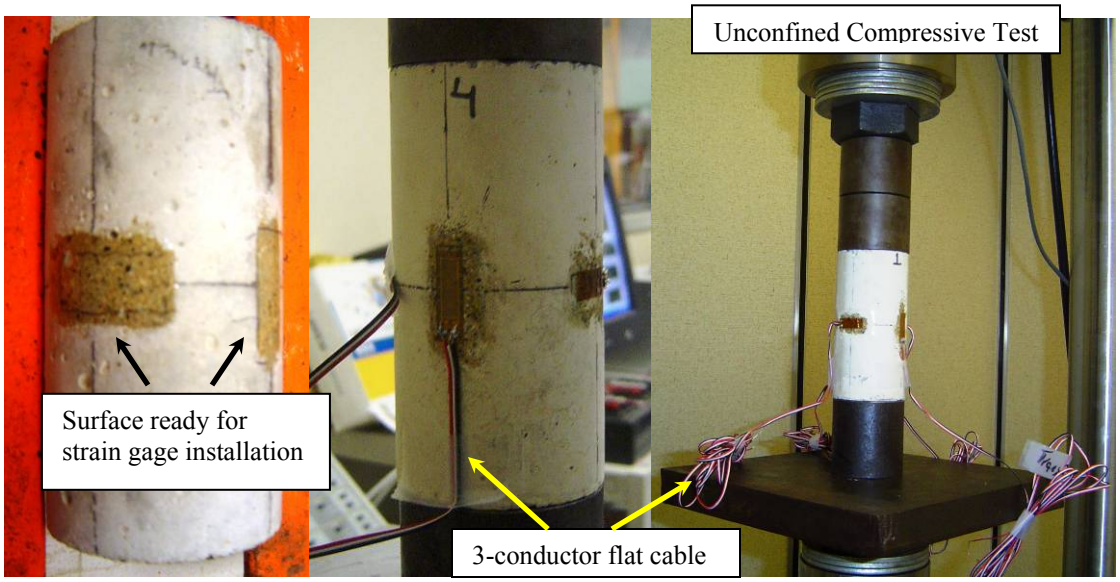


**Figure 3-5: Photos of cylinder preparation for strain gage installation, and unconfined compression test setup**

Specimens used for unconfined compression tests and those used for triaxial compression tests went through the same preparation process. The only difference was the type of lead wires used to connect the strain gages to the data acquisition system. As shown in Figure 3-5, for unconfined compression tests the connection was made with Vishay stranded tinned-copper wire, 3-conductor flat cable with vinyl insulation type 326-DFV.

For the compression tests, which used the Hoek Triaxial cell for the application of lateral confinement, the use of the 3-conductor cable was not possible, at least in the portion inside the Hoek cell. Therefore, for the portion inside the membrane of the Hoek triaxial cell, enamel coated solid copper wires (one for each tab) were used. These small gage solid copper wires were carefully soldered to the strain gage tabs, and protected and kept apart by placing an insulating tape on top of each wire. Once outside the Hoek triaxial cell, the solid copper wires were attached and welded to the conventional 3-conductor flat cable used for the unconfined compression tests. This setup is shown in Figure 3-6. The left photo in Figure 3-6 shows a triaxial compression test specimen ready to be placed inside the confinement membrane and Hoek cell. This picture shows the solid copper wires soldered to each tab of the strain gage. It can be seen that the wires are then taped to the cylinder. Care was taken to keep both copper wires separate to prevent a short circuit during application of the confinement and testing. The photo to the right of Figure 3-6 shows the connection between the two copper wires and the 3-conductor cable. The red cable was soldered onto one of the copper wires; the black and white cables were soldered onto the other copper wire. Figures 3-7 and 3-8 show a close-up of the copper wires soldered onto the connection tabs of a strain gage and of the copper wires soldered onto a 3-conductor cable, respectively.

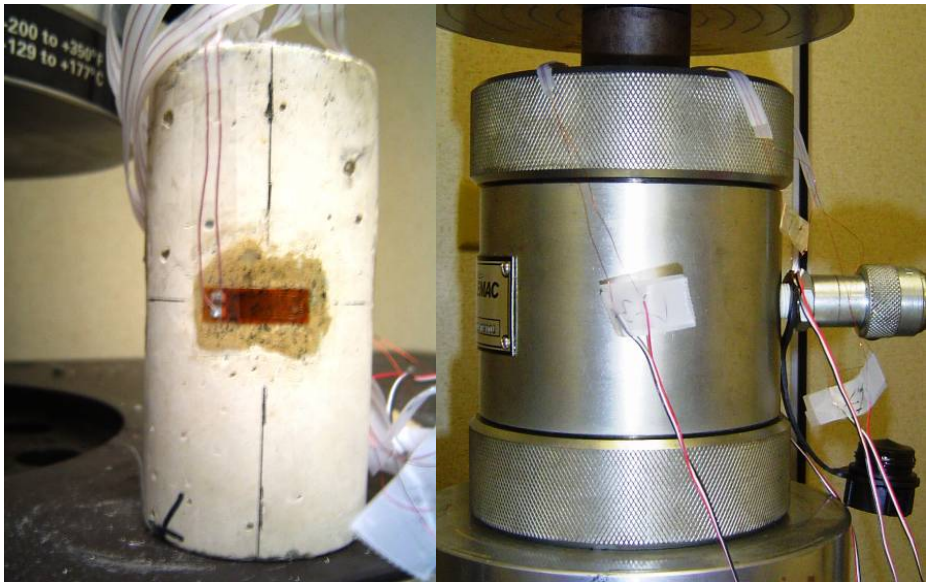

**Figure 3-6: Triaxial compression test cylinder (left); Copper wire / 3-conductor cable connection (right)**

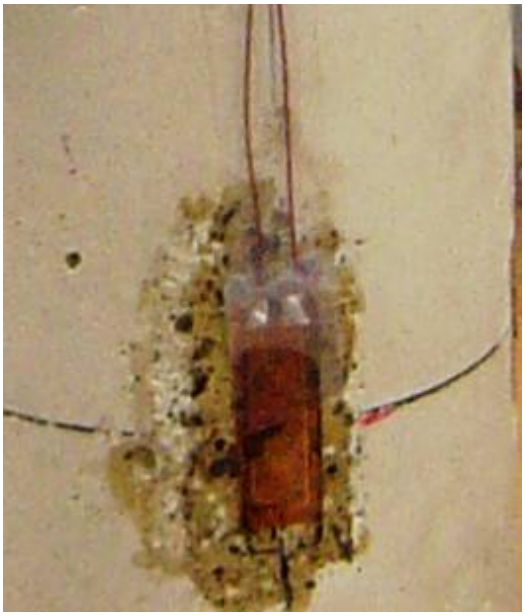

**Figure 3-7: Close-up of a typical copper wire / strain gage CEA-06-500UW-350 connection**

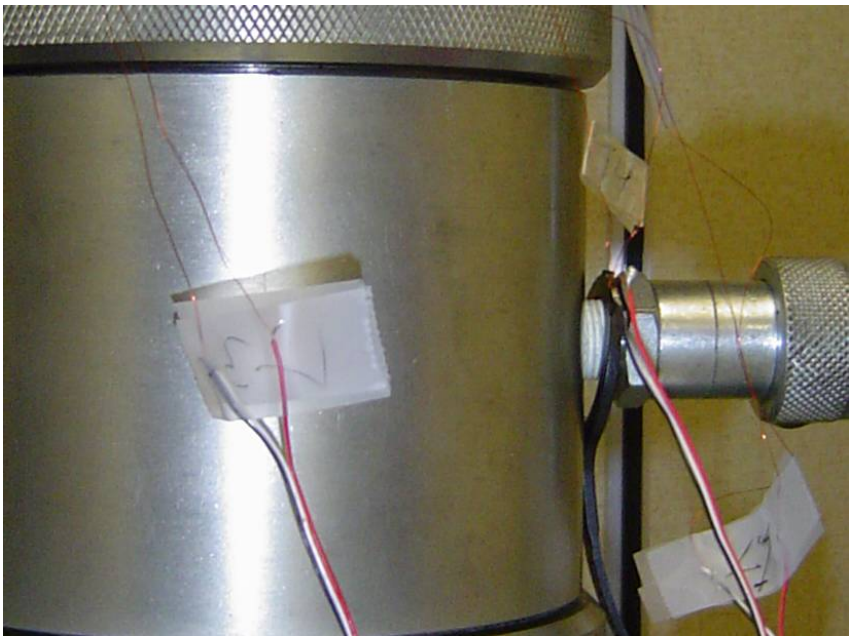

**Figure 3-8: Close-up of a typical copper wire / 3-connector cable connection**

As mentioned before, the triaxial compression tests were carried out using a Hoek triaxial cell model HTC from Roctest, shown in Figure 3-9. Details on this type of triaxial cell device may be found in previously published literature (e.g., Hoek and Franklin, 1968). Figure 3-10 shows a detailed cutaway view of the Hoek triaxial cell

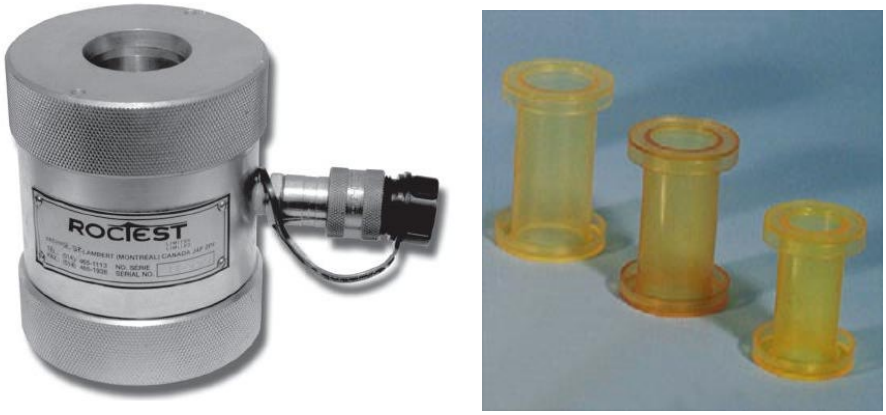


**Figure 3-9: Hoek triaxial cell (left); rubber membrane with U-shaped end seals (right)**

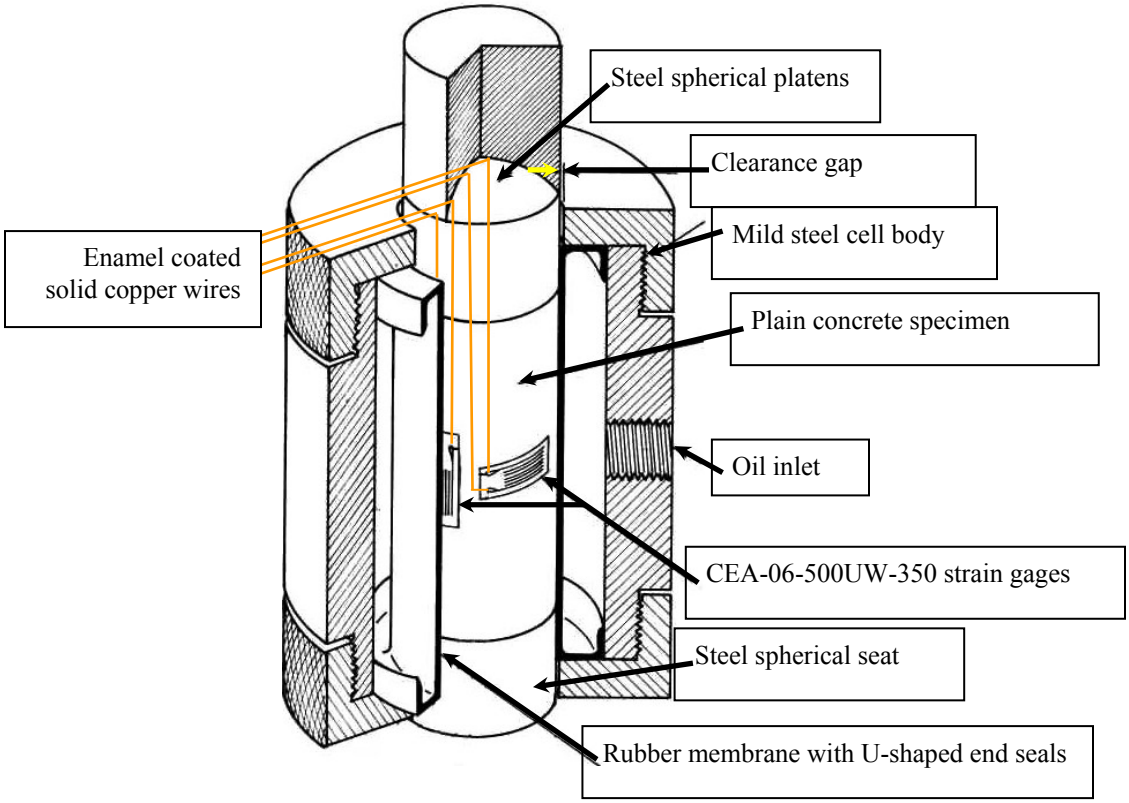


**Figure 3-10: Cutaway view of Hoek triaxial cell (Adapted from Hoek and Franklin, 1968)**

The maximum lateral confining pressure that can be provided by this type of Hoek triaxial cell is 5500 psi (38000 kPa). This level of confinement was deemed sufficient for this research given that the FRP jackets being used in the UPRM concurrent related study could effectively only provide a lateral confinement of about 3200 psi. For this research the confinement level used in the triaxial compression tests was limited to a maximum of 4000 psi (See Table 3-1).

Figure 3-11 shows schematically the test setup used for the triaxial compression tests. To ensure that there was no concentration of forces at the top and/or bottom of the test samples, the ends of each specimen were carefully ground to obtain ends that are parallel and

planar. Spherical platens were used to further ensure proper alignment and axial compression loading.

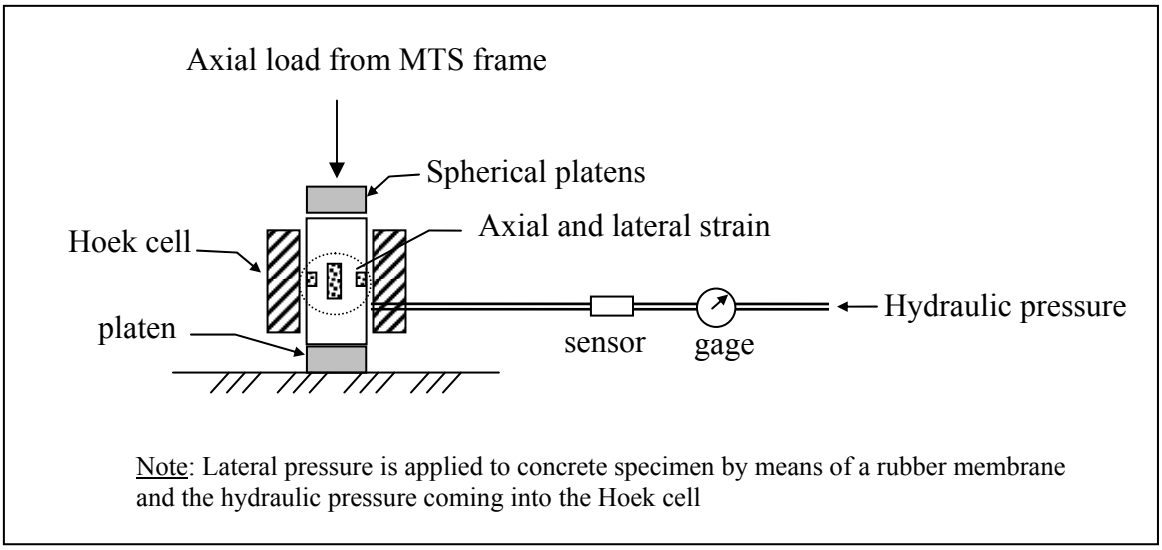


**Figure 3-11: Schematic of Test Setup**

The lateral confining pressure applied by the Hoek cell was achieved by means of hydraulic pressure applied with a hand pump capable of applying a maximum pressure of 10,000 psi. The pressure was monitored visually using a pressure dial gage and also electronically using an Omega PX302 pressure sensor. The complete hydraulic pressure setup is shown in Figure 3-12.

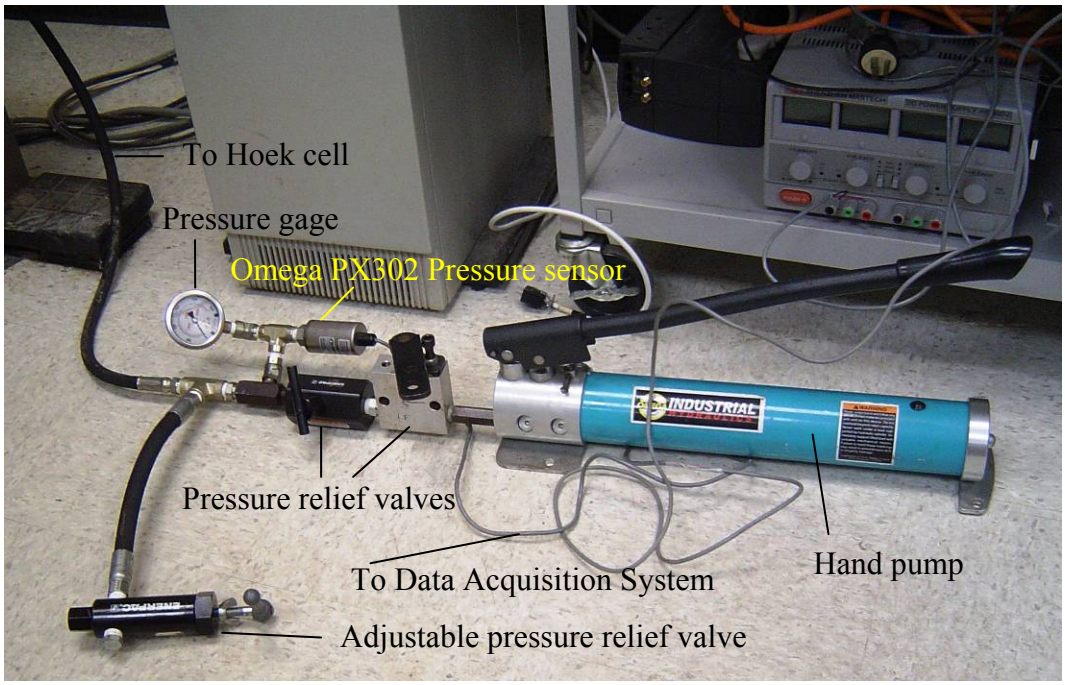


**Figure 3-12: Hydraulic pressure setup for application of triaxial confining pressure**

Triaxial tests were carried out under displacement controlled conditions at a displacement rate of 0.01 inches per minute. This value is within the range of values used in previous investigations. However, previous investigations also show that the speed of loading is not too critical since the concrete response is mainly governed by the level of the confinement pressure.

All the data were collected using a National Instruments SCXI 1000 digital data acquisition system capable of reading 16 input channels and a digital multifunction 12 bit card National Instruments DAQcard™ 6024E. The axial load was measured using a calibrated 55 kip load cell. Axial and lateral deformations were recorded by means of the four 350 Ω Vishay strain gages described before, which, as mentioned, were fixed to the outer wall of the concrete specimen. The confining pressure was recorded by means of the Omega pressure transducer. Axial displacement of the cross head of the MTS system was

also recorded. However, this measurement was not used since it does not provide reliable information due to machine compliance effects. A total of seven input channels were used per test. An eight-channel quick-connect station was used which allowed ease of test setup. Electronic feed for the strain gages, pressure sensor, load cell, and cross-head displacement sensors were provided by the SCXI 1000. The data acquisition system and related setup are shown in Figure 3-13.

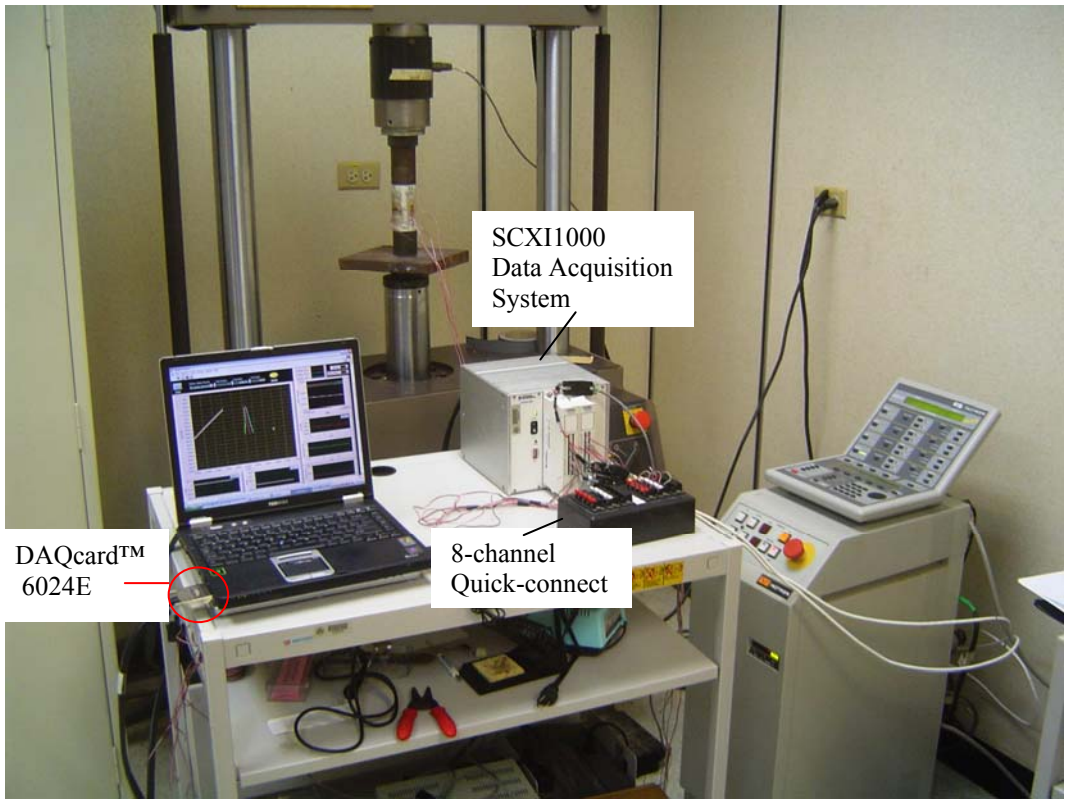


**Figure 3-13: Data acquisition setup**

# CHAPTER 4: EXPERIMENTAL RESULTS

The test matrix presented in the experimental program was designed to study several properties and characteristics of laterally confined plain concrete while axial load was applied. Axial load, longitudinal strain, and hoop strain were recorded during each test. This information was used to create stress-strain plots, study volume change tendencies, and the overall effect the application of confinement stress has on the behavior and characteristics of the concrete.

This chapter presents the experimental results and data analysis obtained from the experimental program carried out for this research project. The data is presented in tabular and/or graphical form and is subsequently discussed in detail.

## 4.1 COMPRESSIVE STRENGTH

The values of maximum compressive strength were obtained by dividing the maximum load reached per test by the specimen cross-sectional area at failure. Table 4-1 lists the average maximum compressive strength, standard deviation, and sample size in each test series.

**Table 4-1: Average maximum compressive strength obtained per test set**

| Test Series | $\sigma_3$ (psi) | $\sigma_{1\ max\text{-}ave}$ (psi) | Std. Dev. (psi) | Sample Size |
|---|---|---|---|---|
| 1 | 0 | 1708 | 199 | 4 |
| 2 | 500 | 4018 | 126 | 3 |
| 3 | 1000 | 5281 | 142 | 3 |
| 4 | 1500 | 6842 | 195 | 3 |
| 5 | 2000 | 9192 | 294 | 3 |
| 6 | 3000 | 12151 | 318 | 3 |
| 7 | 4000 | 15970 | N/A | 1 |

Note that for test series 7, corresponding to a confinement stress of 4000 psi, only one value of maximum axial compressive strength was obtained. This value was read directly from the Instron digital display. Also, for confinement stresses 2000 psi and greater, an increment in standard deviation of the maximum compressive strength was noted. Figure 4-1 shows the maximum compressive strength obtained per test and the average maximum compressive strength.

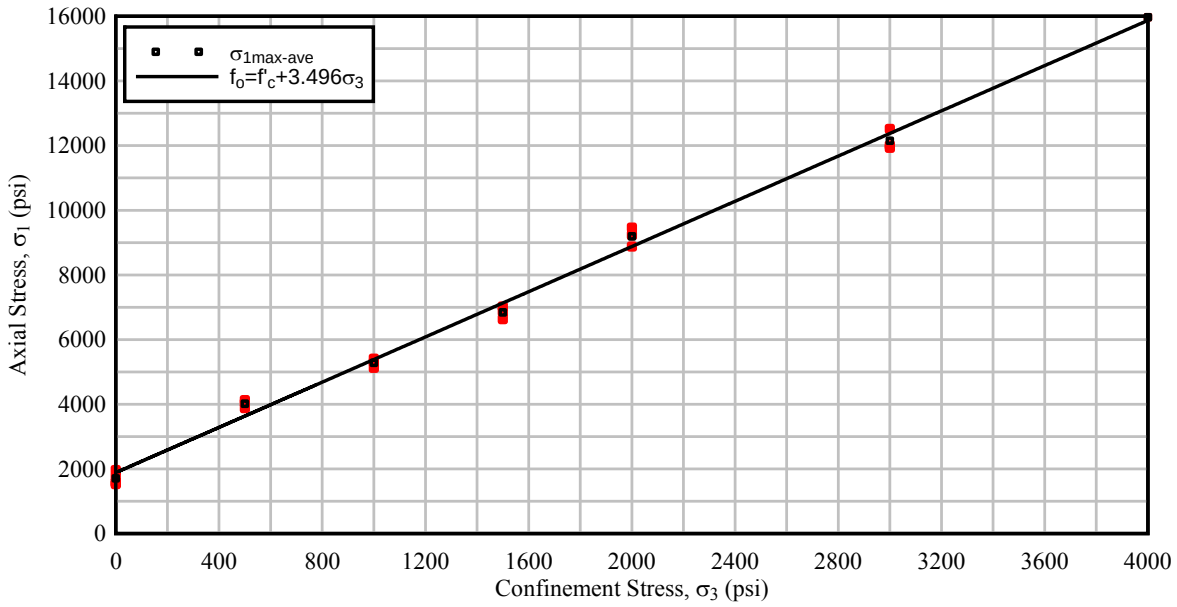


**Figure 4-1: Average maximum compressive strength per confinement level**

Part of the objectives of this research was to determine material parameters of the plain concrete such as cohesion intercept and angle of internal friction. The Mohr-Coulomb failure criterion allows determining these properties from ultimate compressive strength data at various confinement stresses. Figure 4-2 contains the plot of the Mohr circles for each test series. Using this plot, the Mohr-Coulomb failure envelope was graphically generated. From

the plot an empirical angle of internal friction was determined to be approximately 34 degrees; an apparent cohesion of approximately 435 psi was also measured.

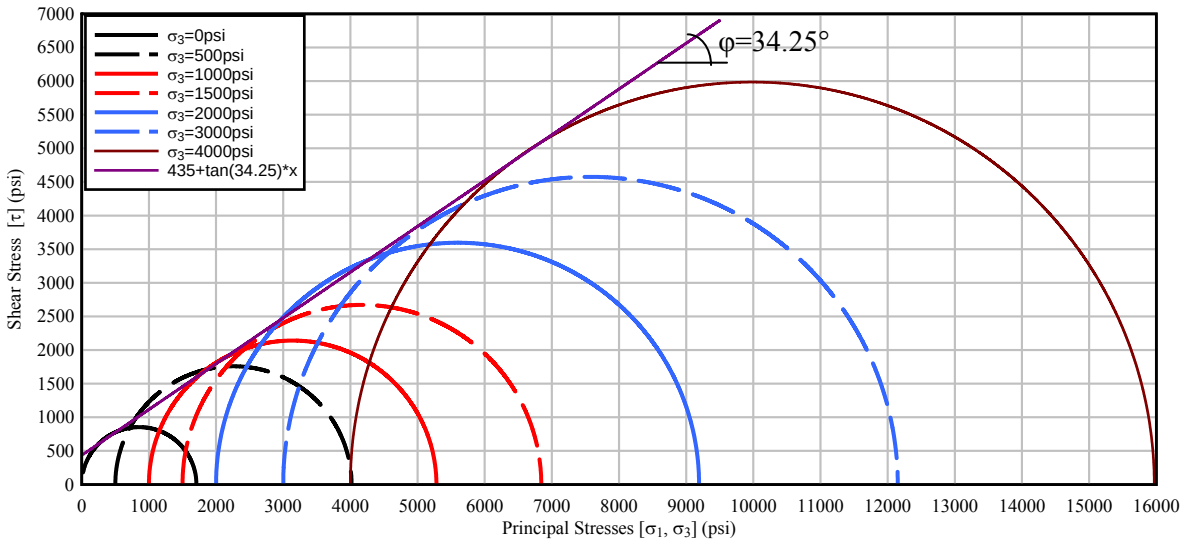


**Figure 4-2: Mohr-Coulomb failure envelope for the unreinforced plain concrete studied**

## 4.2 STRESS-STRAIN CURVES

Other objective of this research was to investigate the stress-strain behavior of plain concrete specimens subjected to triaxial compression. This section presents an analysis of the results from unconfined compressive and triaxial compression tests conducted on the plain concrete specimens.

Unconfined compressive strength data were obtained from four tests. The stress-strain curves from the four tests are plotted in Figure 4-3. The stress-strain curves obtained were reasonably close with average peak strength of 1708 psi.

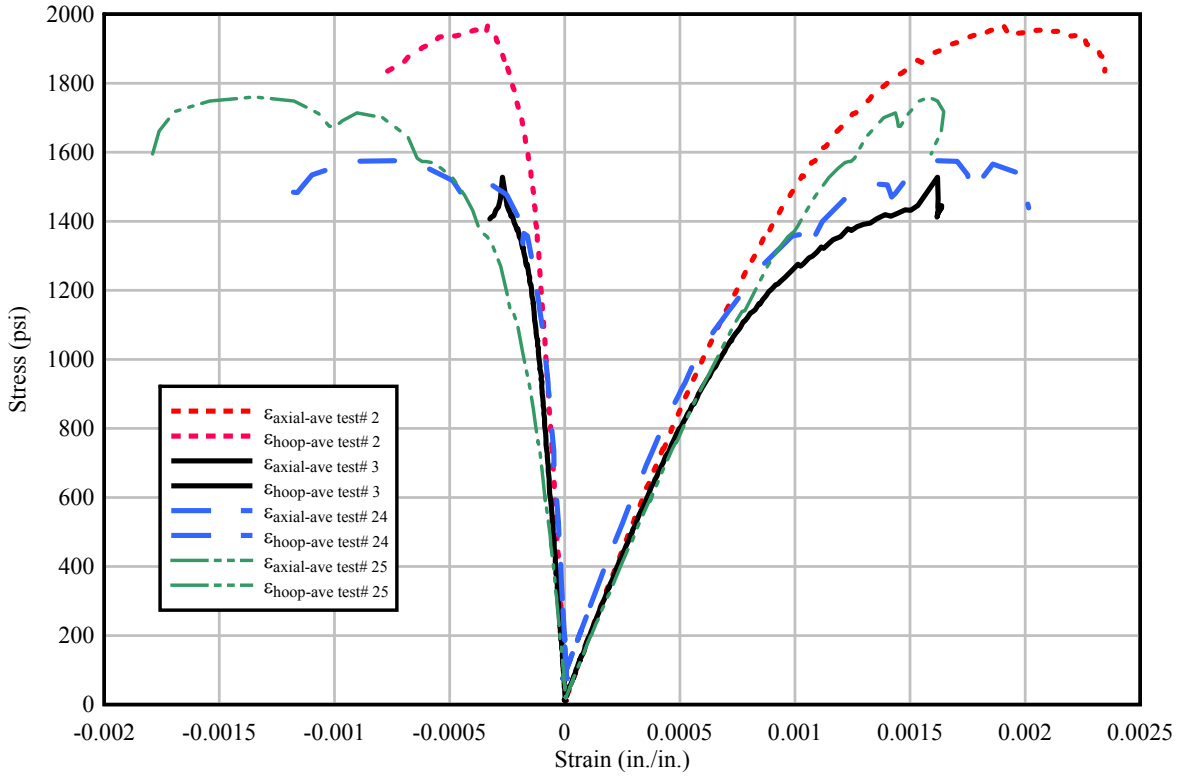


**Figure 4-3: Stress-strain curves from Unconfined Compressive tests**

The unconfined compressive stress-strain curves obtained in this research were compared with the curves obtained by Dávila (2007), who tested samples prepared from the same concrete batch. The samples tested by Dávila (2007) were 6 inches in diameter and 12 inches in height. Besides testing larger samples, the tests by Dávila (2007) involved specimens cured under similar conditions but were tested at an age of 52 days and the test device used was a Forney LT 1000-03, which is a stress controlled system. Dávila's tests were carried out at a load rate of 67 pound-force per second. In comparison, the tests for this research were strain controlled at a displacement rate of 0.01 inches per minute. Figure 4-4 compares the stress-strain curves obtained in this research with those from Dávila (2007).

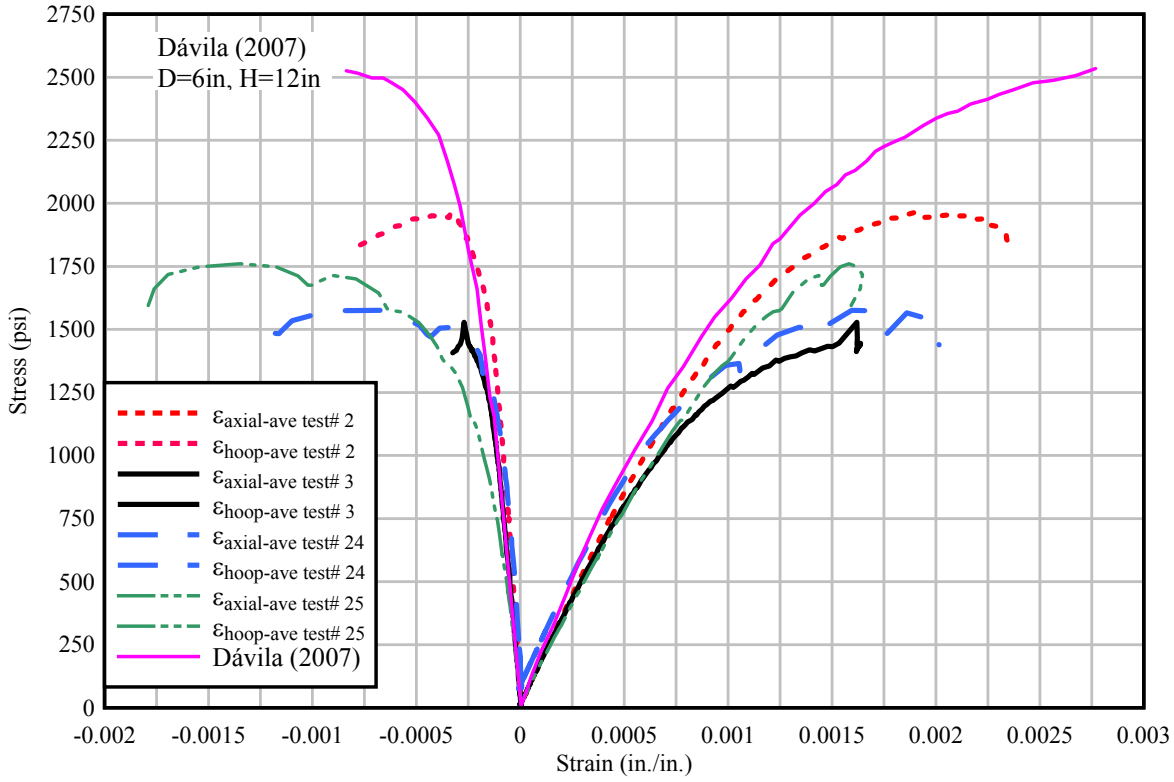


**Figure 4-4: Comparison plot of stress-strain curves from Unconfined Compressive tests by Dávila and those obtained in this research**

In general, the curves by Dávila (2007) exhibit the same stress-strain behavior as those from this research. This is particularly true for the initial portion of the curves. Hoop strain at failure is within the values obtained in this research, while axial strength and axial strain at failure are somewhat higher than those obtained in this research. This is consistent with the findings of Issa et al. (2000), who concluded that when comparing geometrically similar specimens, the larger samples will exhibit a higher compressive strength.

Triaxial compressive strength data were obtained from three tests per confinement level. The stress-strain curves from the three tests are plotted for each confinement level in Figures 4-4 through 4-10. Figure 4-11 presents a compilation of all the stress-strain curves

for all the test series, allowing a visual grasp of the effect that confinement pressure has on stress and strain at failure, as well as general material behavior during loading and at failure.

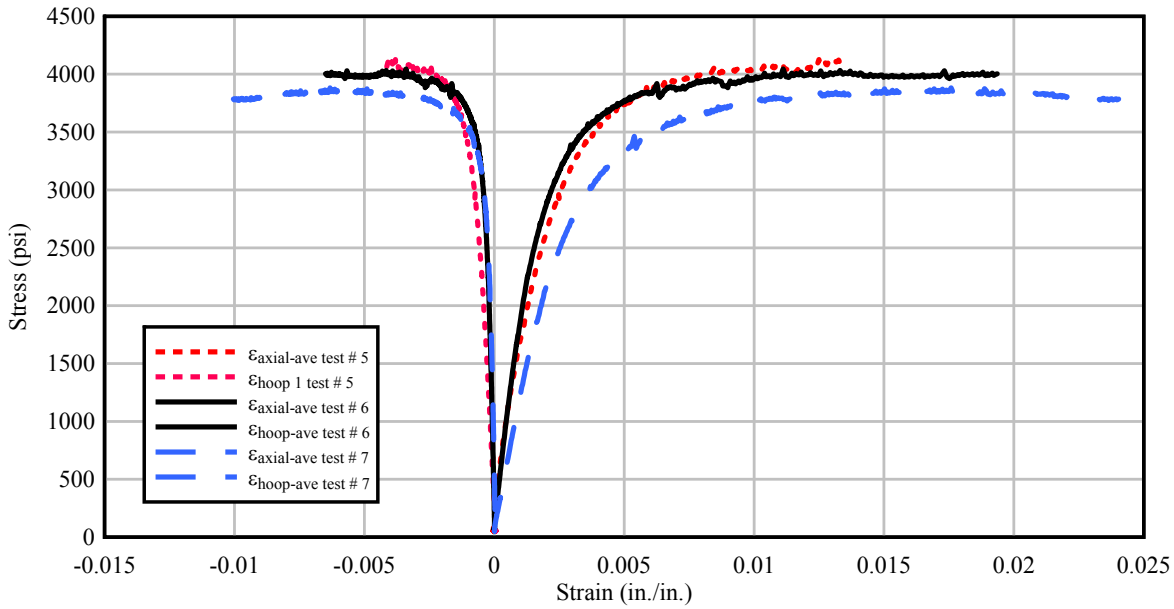


**Figure 4-5: Stress-strain curves from triaxial tests at a confining pressure of 500 psi**

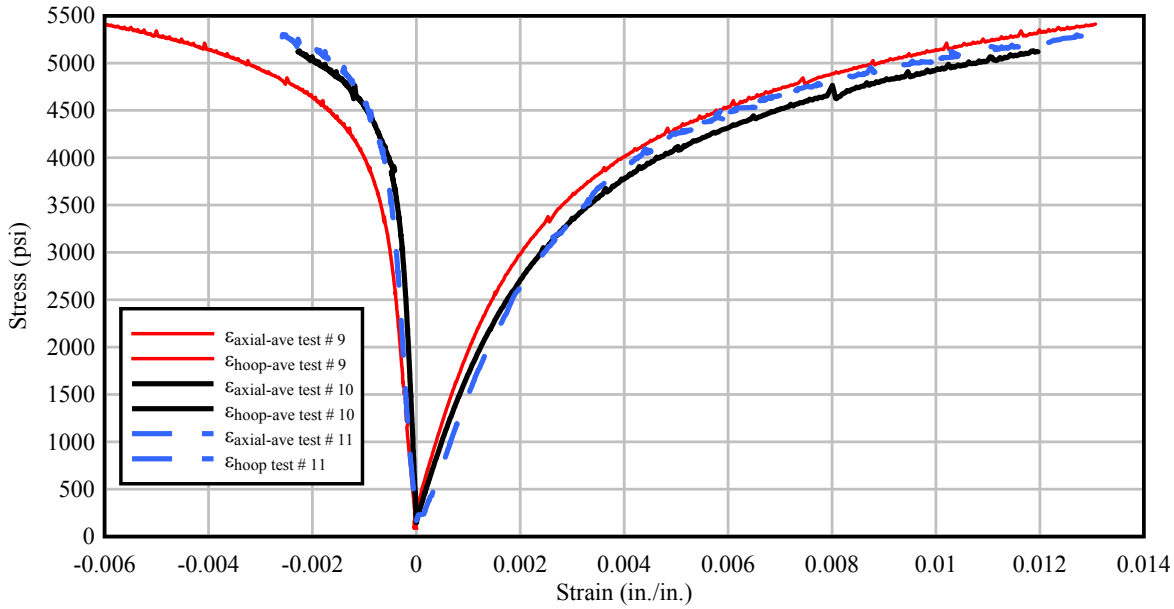


**Figure 4-6: Stress-strain curves from triaxial tests at a confining pressure of 1000 psi**

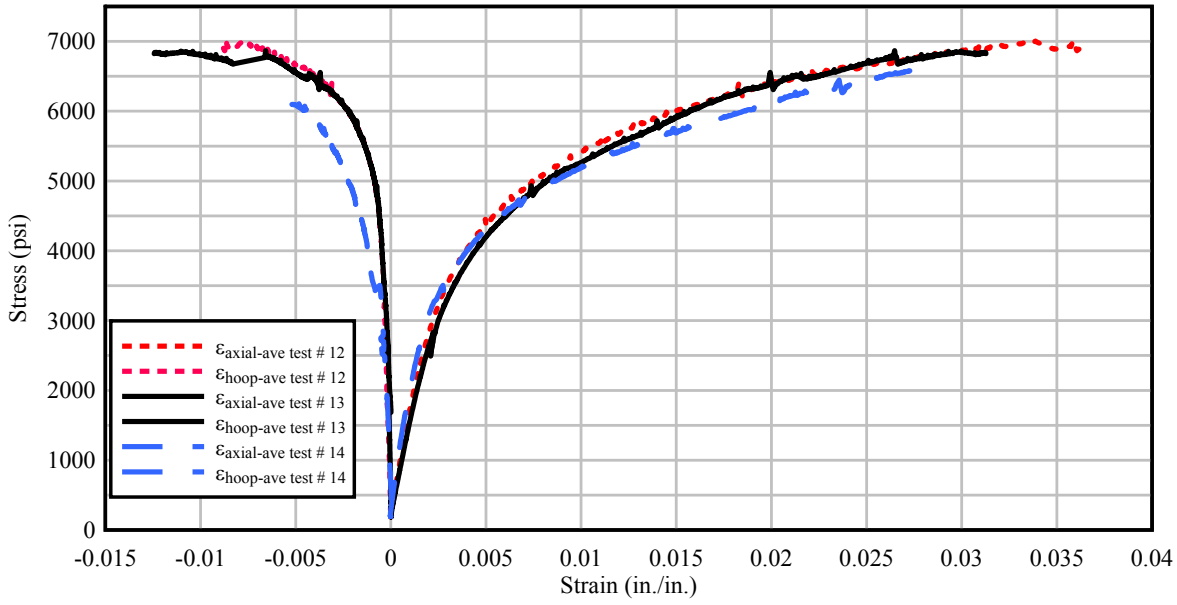


**Figure 4-7: Stress-strain curves from triaxial tests at a confining pressure of 1500 psi**

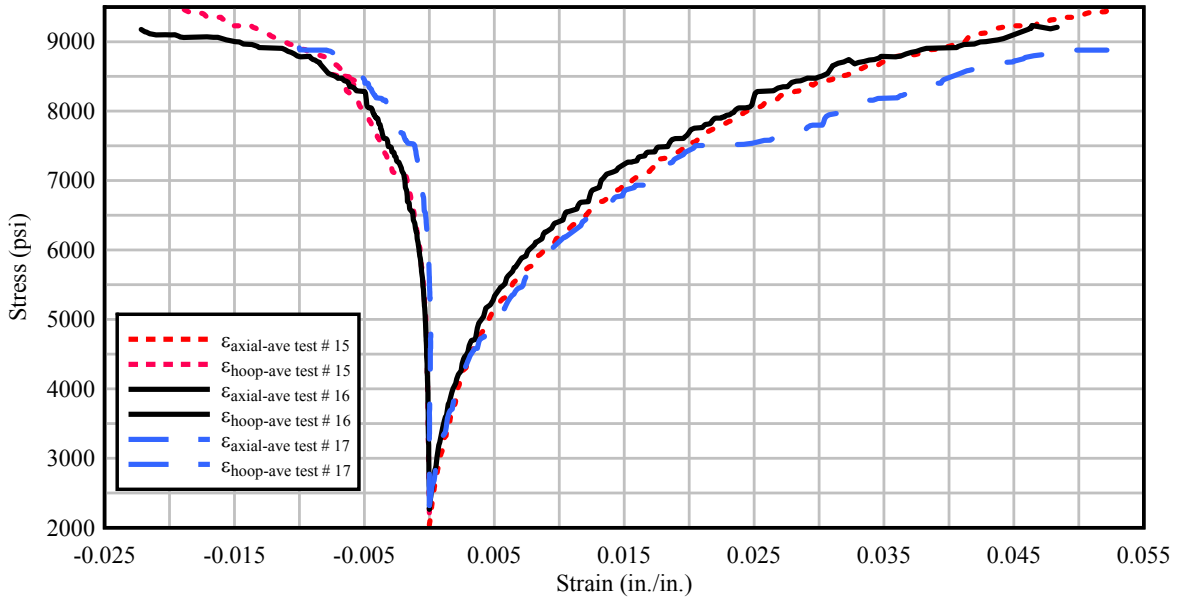


**Figure 4-8: Stress-strain curves from triaxial tests at a confining pressure of 2000 psi**

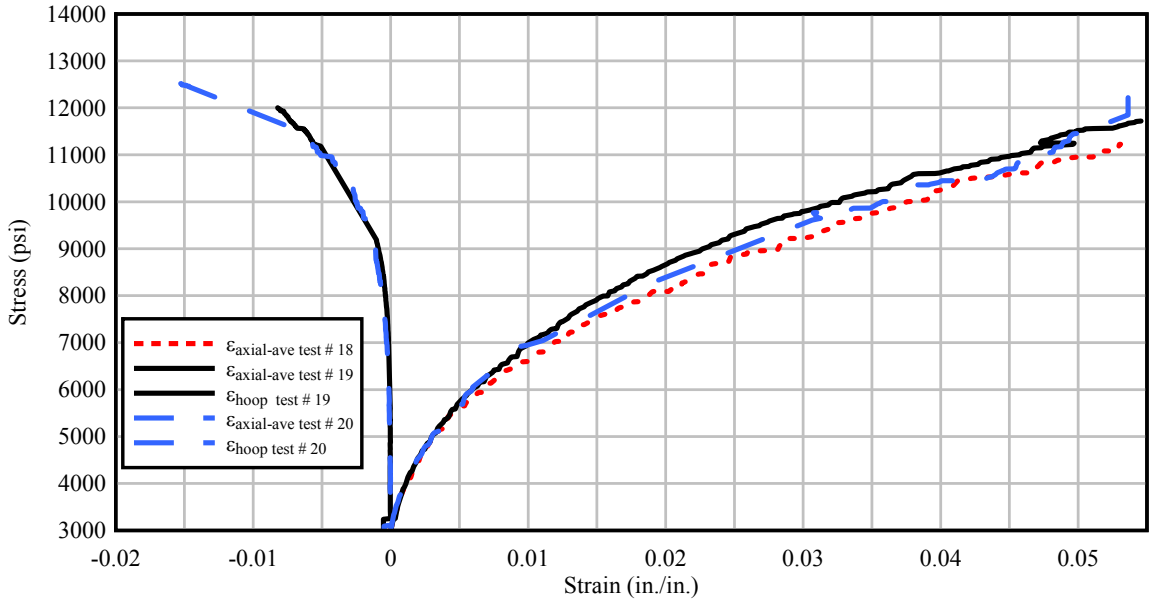


**Figure 4-9: Stress-strain curves from tests at a confining pressure of 3000 psi**

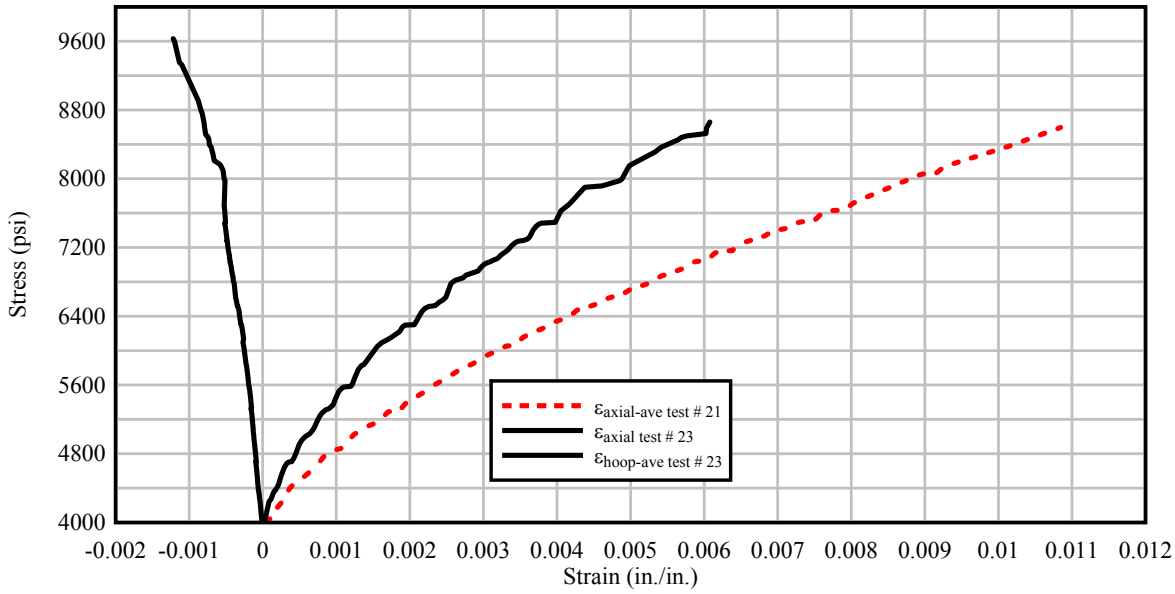


**Figure 4-10: Stress-strain curves from tests at a confining pressure of 4000 psi**

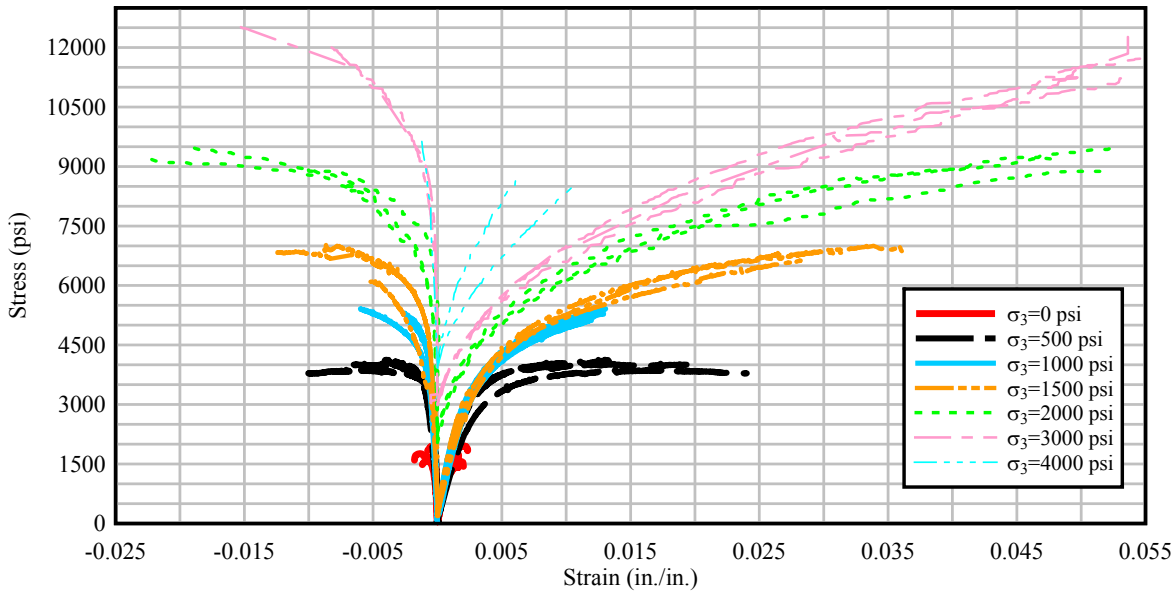


**Figure 4-11: Comparison plot of stress-strain curves from all tests series**

A few comments should be made concerning the way load was applied to the plain concrete specimens. For all tests where the confinement pressure was 1500 psi or lower, confinement pressure was applied and maintained constant prior to the application of axial load under displacement control, in a manner consistent with traditional triaxial tests (Imran and Pantazopoulou 1996). For all tests where the confinement pressure was 2000 psi or higher, confining pressure was increased in a stepwise manner, alternating with a stepwise increase of the axial load (Imran and Pantazopoulou 1996). This was done to prevent exceeding the specimen's compressive strength and causing failure prior to the full application of the confining pressure. This procedure is also in accordance with ASTM C801-98. Note that for all the tests where a stepwise increment in load and confining pressure was followed ($\sigma_3 \geq 2000$ psi), the axial stress takes into account the initial hydrostatic

pressure (i.e. $\sigma_1=\sigma_3$) and therefore the stress-strain curves do not begin from zero but from the value of the confining pressure (Sfer et al. 2002)

A few comments should also be made concerning the use of strain gages inside a rubber membrane at high confinement pressures. Strain gage data were extremely difficult to obtain for the tests where the compressive stress was 3000 psi or higher. In several instances the strain gages transmitted data during the initial part of a test and then failed, causing the data acquisition system to freeze. On other occasions, the strain value would suddenly increase or decrease violently indicating that a short circuit of the connecting wires had occurred or that the gages had detached from the sample. Figure 4-10 illustrates how few data points were captured from triaxial tests at a confining pressure of 4000 psi due to strain gage failure. This test series was not repeated due to a limited quantity of test specimens. It is recommended that for future testing a hinged ring lateral deformeters and a linear potentiometer be used for radial and axial displacements, respectively.

Figure 4-11 contains the stress-strain curves from all tests series. This plot shows the effects of confinement on the stress-strain behavior of the plain concrete studied in this research. Note that at a given strain, the compressive strength of the plain concrete increases significantly. The stress-strain curves from the unconfined compression tests exhibit a well-defined peak load and a rapid post-peak descent. The stress-strain curves from the triaxial tests exhibit an increase in the peak load, and a decrease in the steepness of the post-peak response with an increase in the lateral confinement pressure. This indicates an increase in ultimate axial stress and ductility of the plain concrete with confinement (Sfer et al. 2002). The decrease in slope of the post-peak response with an increase in the lateral confinement pressure indicates that a transition from brittle to ductile failure occurs. The confinement

pressure acts as a delay mechanism for the development of macrocracks in the specimen. At higher confinement pressures the softening and degradation of the compressive strength of the plain concrete is reduced, because of this, a plateau in the post-peak regime of the stress-strain curves from the triaxial tests develops (Imran and Pantazopoulou 1996).

An average initial tangential modulus was determined for the plain concrete for each test series. The modulus was calculated from the initial slope of the axial stress-strain curve between 100 and 1000 microstrains of axial deformation for each test. Note that the initial tangential modulus is not the modulus of elasticity, except for the unconfined compressive strength test curves (Sfer et al. 2002). Figure 4-12 presents the average initial tangential modulus per confinement level.

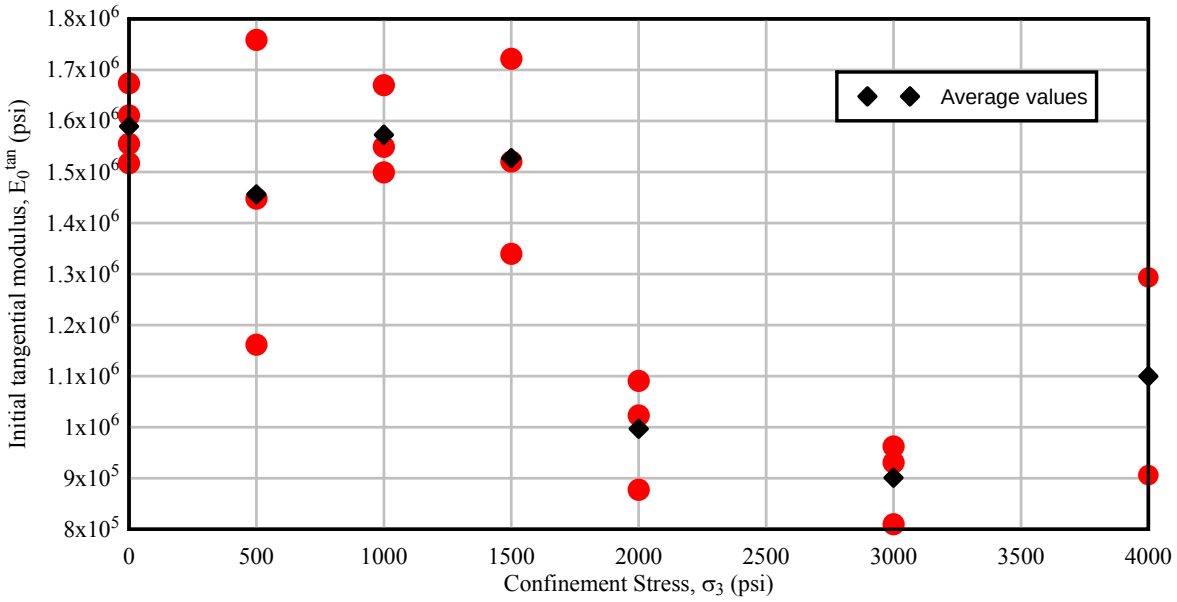


**Figure 4-12: Average initial tangential modulus per confinement level**

The data presented in Figure 4-12 show that the elastic behavior of plain concrete is improved by confinement pressure. The scatter in the data set is too large to generate an

accurate empirical correlation of the effect of confinement on the specimen's initial tangential modulus. In general terms, the value of the modulus tended to decrease as confinement pressures were increased, i.e. ductility of the plain concrete improved as confinement pressures applied to the specimens were increased. The progressive decrease in the initial slope of the stress-strain curves is in accordance with the results of previous researchers such as Dahl (1992).

Improvement of the ductility of the plain concrete as confinement pressures applied to the specimens were increased is also evidenced in Figure 4-13, where axial strain to failure per confinement level is presented.

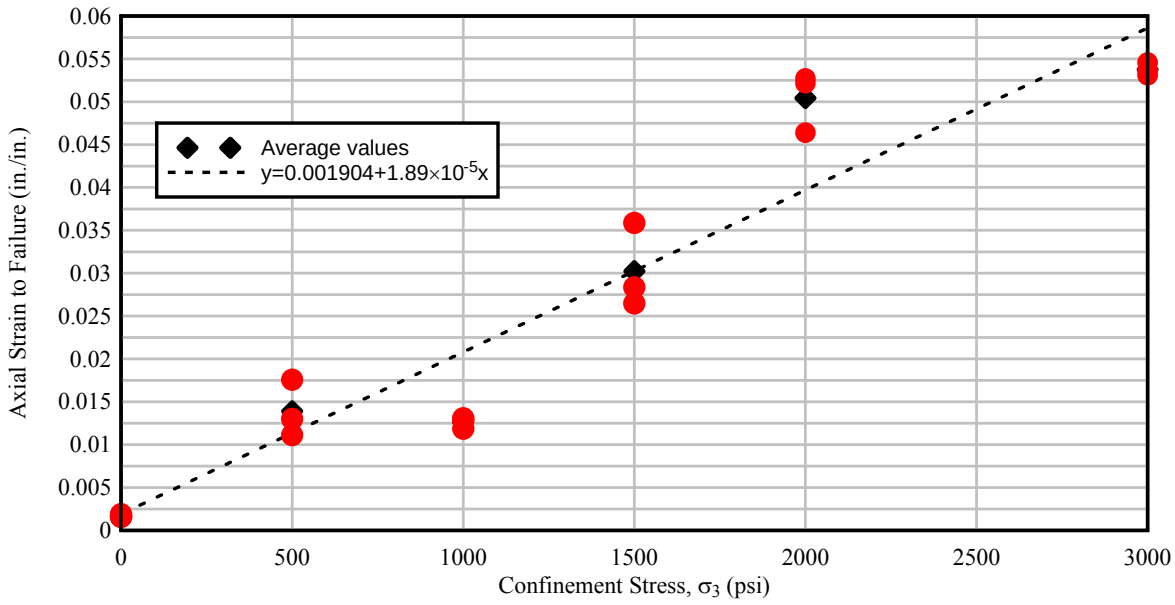


**Figure 4-13: Axial strain to failure per confinement level**

Figure 4-13 shows that, although there is some amount of scatter in the data, a fairly representative linear relationship can be established for the effect an increment in confinement pressure had on ultimate axial strain (ductility) for the plain concrete studied.

Average ultimate axial strain increased from 0.00168 to 0.0538. The data show that the peak strain is more than 30 times higher at the highest level of confinement.

Figure 4-14 presents hoop strain to failure per confinement level. The application of lateral confinement while axially loading the plain concrete specimens also improved lateral ductility of the material, as shown in Figure 4-14.

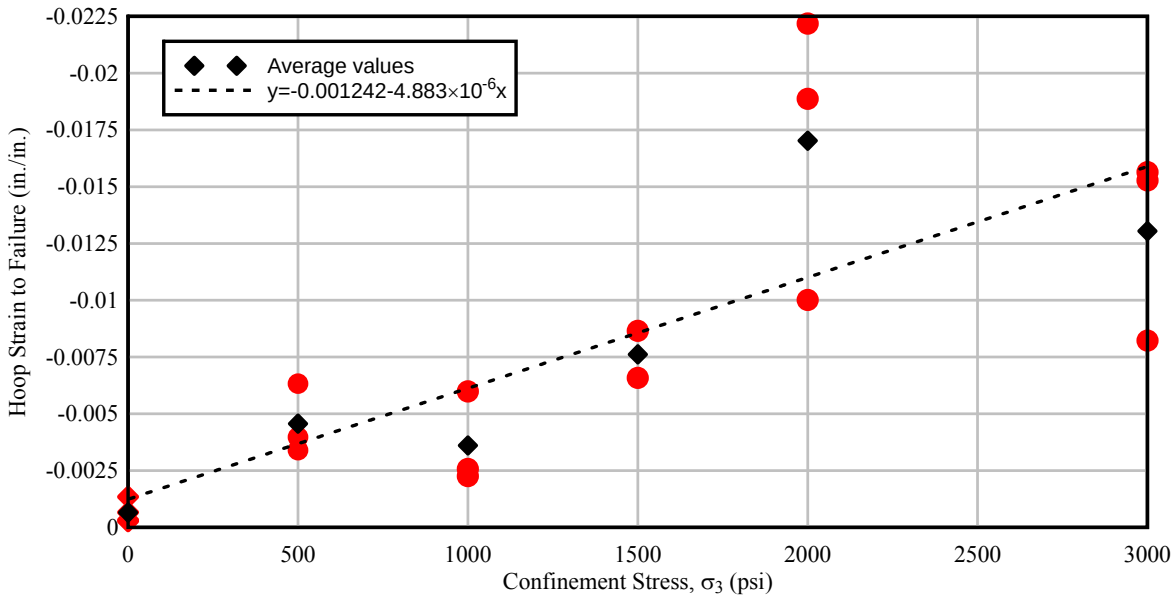


**Figure 4-14: Hoop strain to failure per confinement level**

The figure also shows that, although there is some amount of scatter in the data, a representative linear relationship can be established for the effect an increment in confinement pressure had on ultimate hoop strain for the plain concrete studied. Average ultimate hoop strain increased from -0.000654 to -0.0130. The data show that the peak strain is about 20 times higher at the highest level of confinement.

Figures 4-15 through 4-19 present the variation of the instantaneous Poisson's ratio during the application of constant lateral confining pressure while increasing axial load until failure. The red, blue, or green points represent a single data point in each test. The solid

black line represents the average instantaneous Poisson's ratio at any given normalized axial stress. The solid red line represents the best estimate for the value of the Poisson's ratio in the elastic regime for each test series.

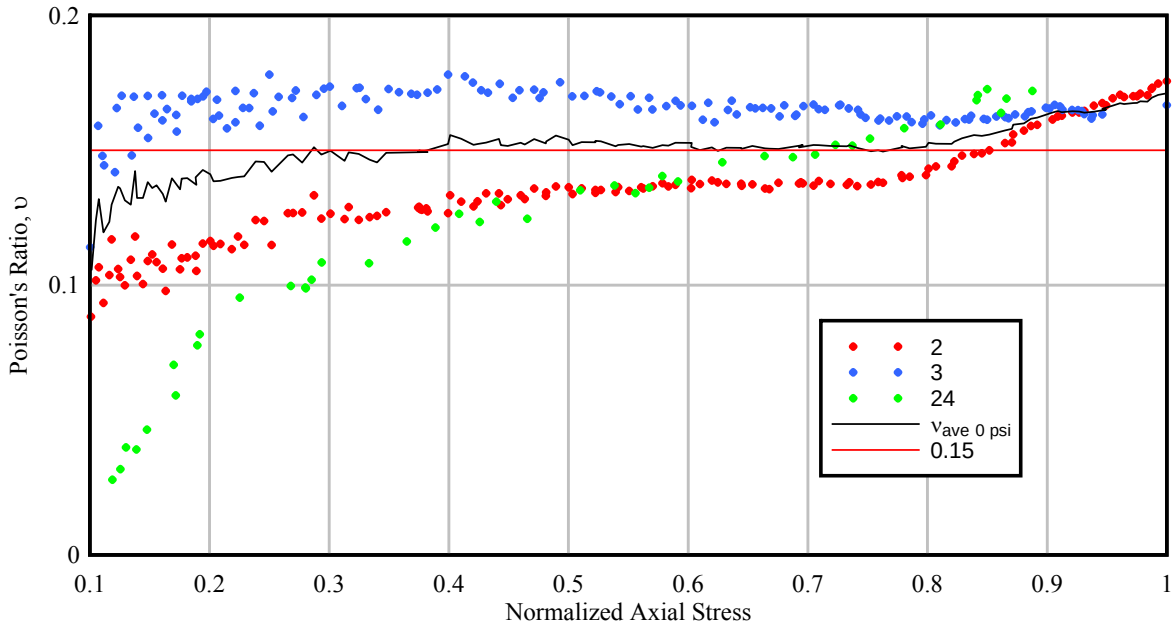


**Figure 4-15: Variation of instantaneous Poisson's ratio during application of axial load with no lateral confinement**

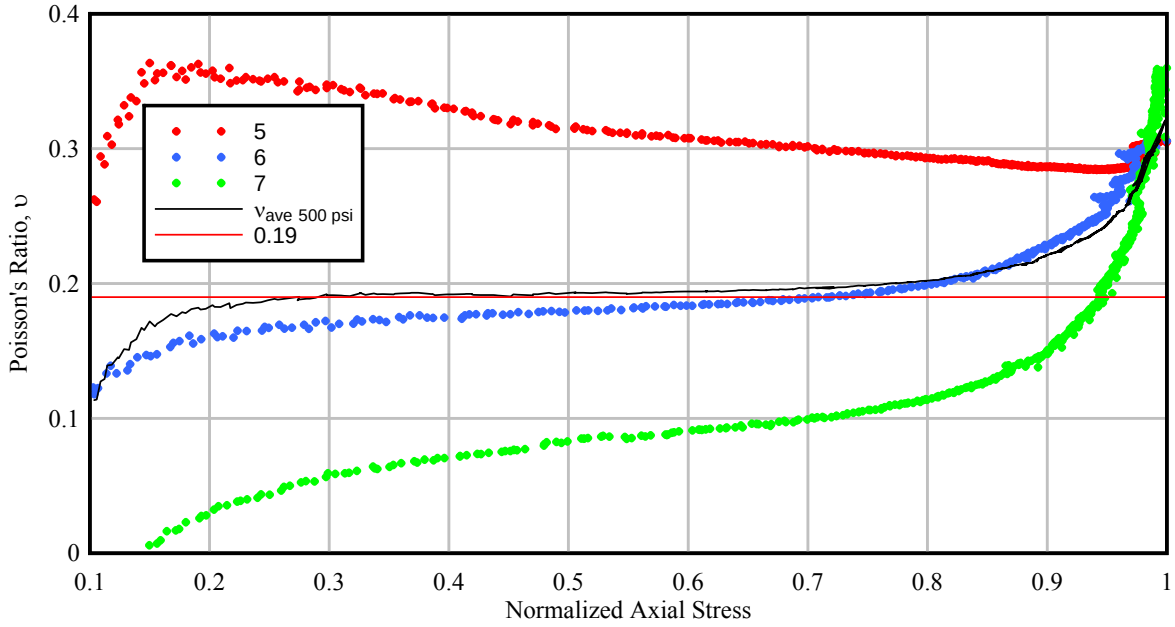


**Figure 4-16: Variation of instantaneous Poisson's ratio during application of axial load with 500 psi lateral confinement**

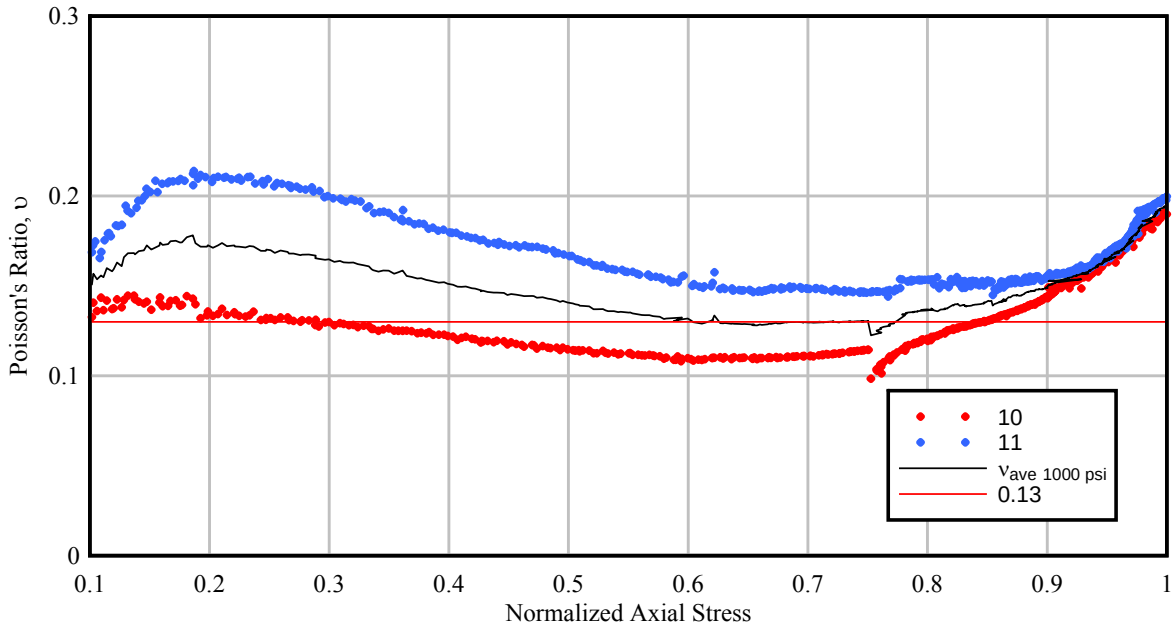


**Figure 4-17: Variation of instantaneous Poisson's ratio during application of axial load with 1000 psi lateral confinement**

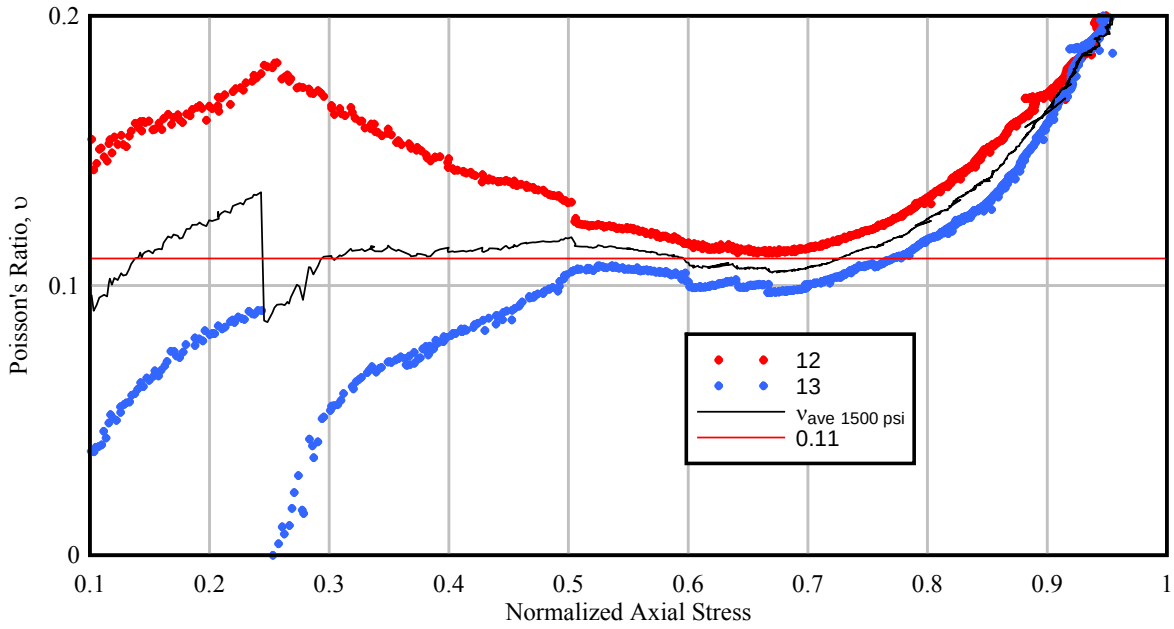


**Figure 4-18: Variation of instantaneous Poisson's ratio during application of axial load with 1500 psi lateral confinement**

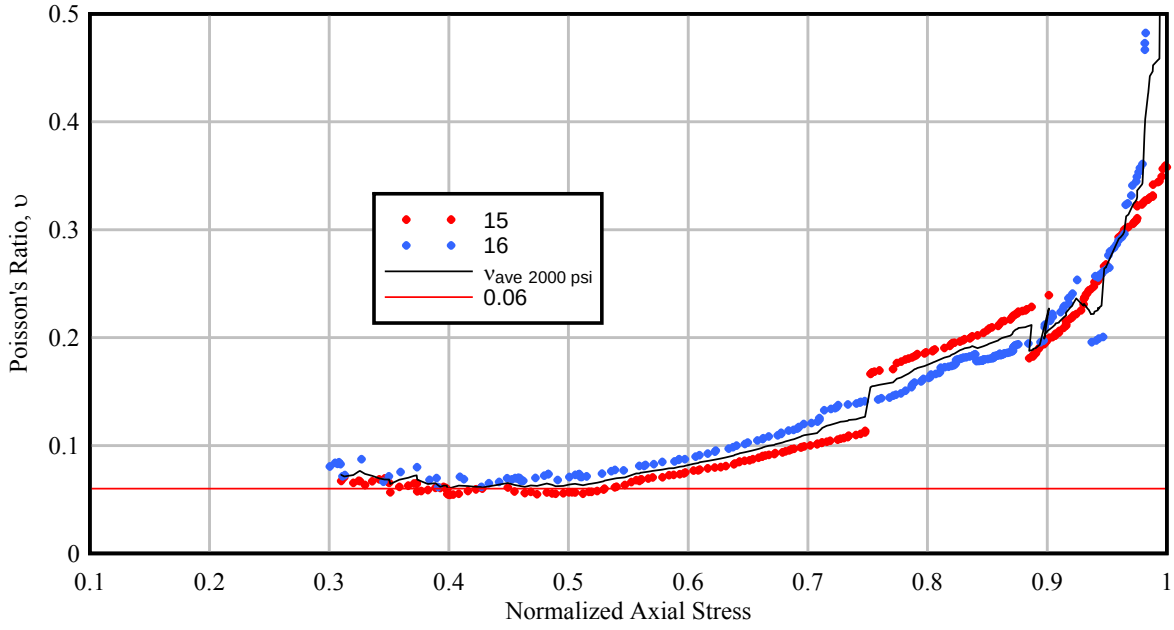


**Figure 4-19: Variation of instantaneous Poisson's ratio during application of axial load with 2000 psi lateral confinement**

# CHAPTER 5: COMPARISON BETWEEN EXPERIMENTAL RESULTS AND EMPIRICAL FORMULATION

This chapter presents a comparison between the values for the material parameters determined through this experimental effort and those predicted by empirical and analytical formulations found in published literature for the plain concrete studied. The axial stress - axial strain curves are also compared to those predicted by the Attard and Setunge (1996) model.

Compressive strength of the plain concrete tested in this research increased as the lateral confinement provided during testing was increased, which is in accordance with published literature. Figure 4-1, Average maximum compressive strength per confinement level, shows the maximum compressive strength obtained per test and the average maximum compressive strength. In order to compare the experimental values obtained with those predicted by existing empirical models, the curves obtained with the following models: Considere (1906); Richart et al. (1928); Tan and Sun (2006) are included in the same plot with the experimental results in Figure 5-1.

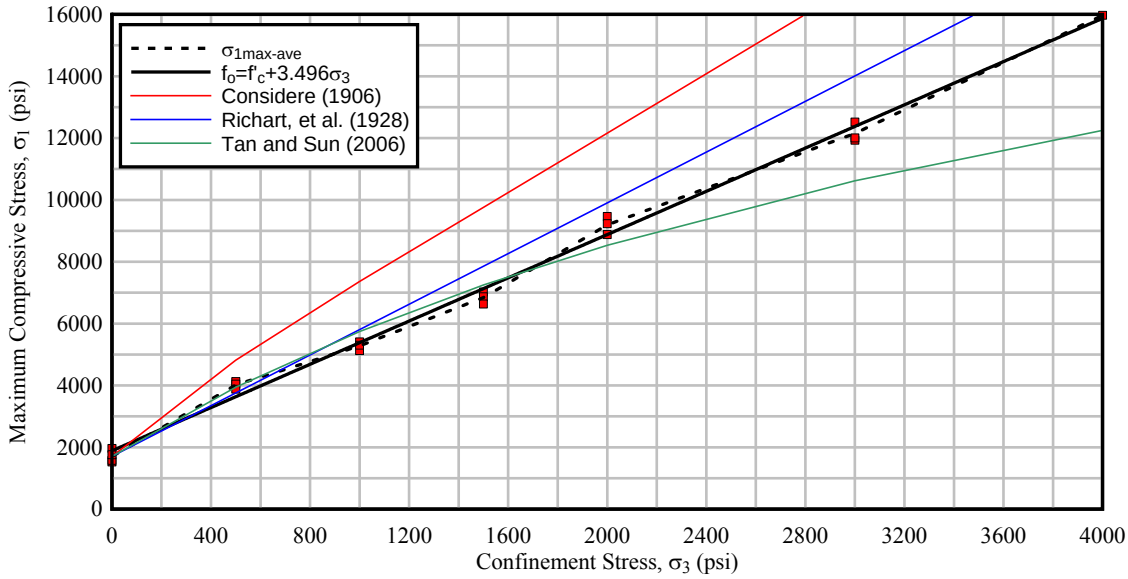


**Figure 5-1: Comparison of compressive strength results with previously published empirical models**

The experimental data in Figure 5-1 show similar trends as the predictions by the empirical models. The main difference between the linear correlation established in this research and the models by Considere and Richart et al. is the confining stress multiplier. It could be argued that the difference in this multiplier is due to the use of different sample sizes, mix designs, and unconfined compressive strengths in each research effort. The Tan and Sun model agrees well with the experimental data up to 2000 psi of confining pressure. At higher confining pressures the model predicts a non-linear increment in compressive strength at higher lateral pressures. The scope of the data from this research effort did not identify the extent of this nonlinearity. Tan and Sun also note in their research that for concrete under active confinement, concrete with different uniaxial compressive strength will result in different failure envelopes.

The modulus of elasticity for the plain concrete studied was approximately 1,590,000 psi. The value for this modulus determined as specified in ACI 318 is approximately

1,920,000 psi. It is well recognized that the empirical formula for the modulus of elasticity of concrete as published in ACI 318 is only approximate and accurate to plus / minus 20 percent for normal strength concrete. This is due to the modulus' dependence on the type of aggregate used within the mix and the proportion (Attard and Setunge, 1996). The value of the modulus of elasticity obtained experimentally is within the 20 percent accuracy range of the theoretical value and therefore in agreement with the empirical formula.

The data presented in Figure 4-12, average initial tangential modulus per confinement level, show that the elastic behavior of plain concrete is improved by confinement pressure. Improvement of the ductility of the plain concrete as confinement pressures applied to the specimens were increased is also evidenced in Figure 4-13, where axial strain to failure per confinement level is presented. Axial strain to failure increased an order of magnitude from the unconfined test to 3000 psi confinement pressure.

Figure 5-2 compares the values of axial strain to failure obtained with the empirical formulae proposed by Attard and Setunge (1996) to the axial strain to failure results obtained. The strain at peak uniaxial compression (axial strain to failure at no confinement stress) was determined using the gravel aggregates formula.

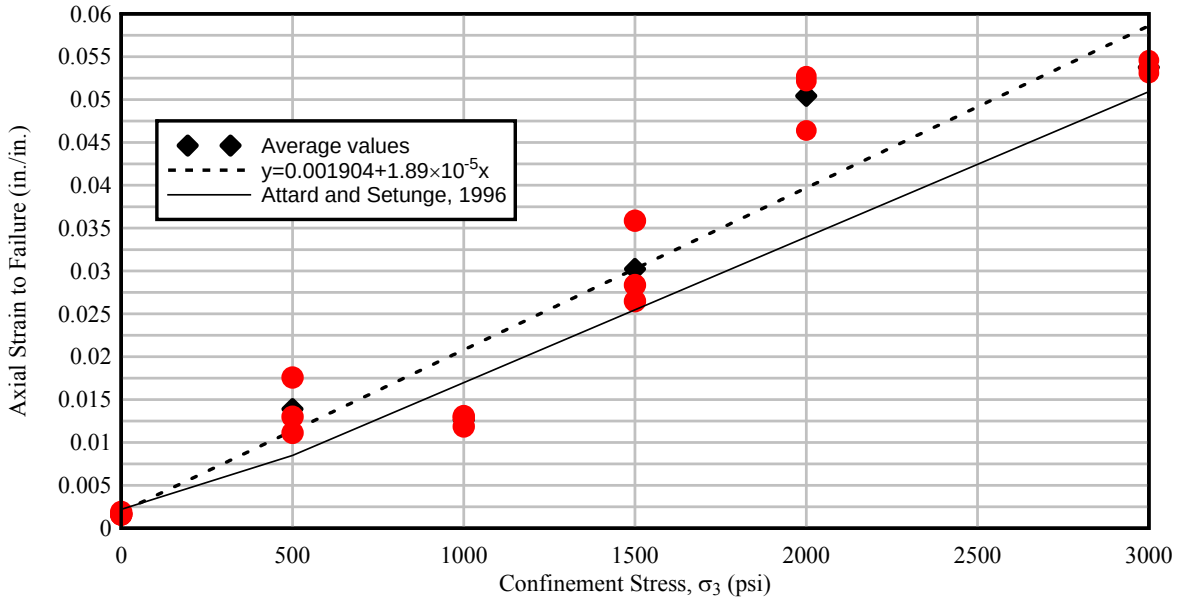


**Figure 5-2: Comparison of axial strain to failure with previously published empirical model**

In general, the experimental results obtained in this research show an agreement in the incremental trend of axial strain to failure with increasing confinement stress. The discrepancy in the values predicted by the formulae and the experimental values obtained is because of the differing types of aggregates used in each research (Attard and Setunge, 1996).

According to Gardner (1969), the experimental results of axial stress against instantaneous Poisson's ratio lie on two straight lines, while for stresses below 80 percent of the ultimate stress the experimental results lie on a straight line. Gardner then states that at failure it appears that the ultimate stress is independent of the instantaneous Poisson's ratio. When comparing his findings to the curves shown in Figure 5-3, it is evident that for all the curves, this theory applies. The effect of lateral confinement on the instantaneous Poisson's ratio at failure is reflected as an increment, not only within each test series, but when

compared to each other. At zero confinement, the curve remains fairly linear. Comparison of the instantaneous Poisson's ratio at failure for 0, 1000, 1500, and 2000 psi permits the conclusion that an increment in confining pressure will increase the ratio at failure. The fairly linear nature of all the curves below 80 percent of the ultimate stress suggests that the confinement has little or no effect on ductility until the development of cracks within the specimen, while the plain concrete displays an almost plastic behavior, large increases in strain and instantaneous Poisson's ratio with little to no increase in axial stress.

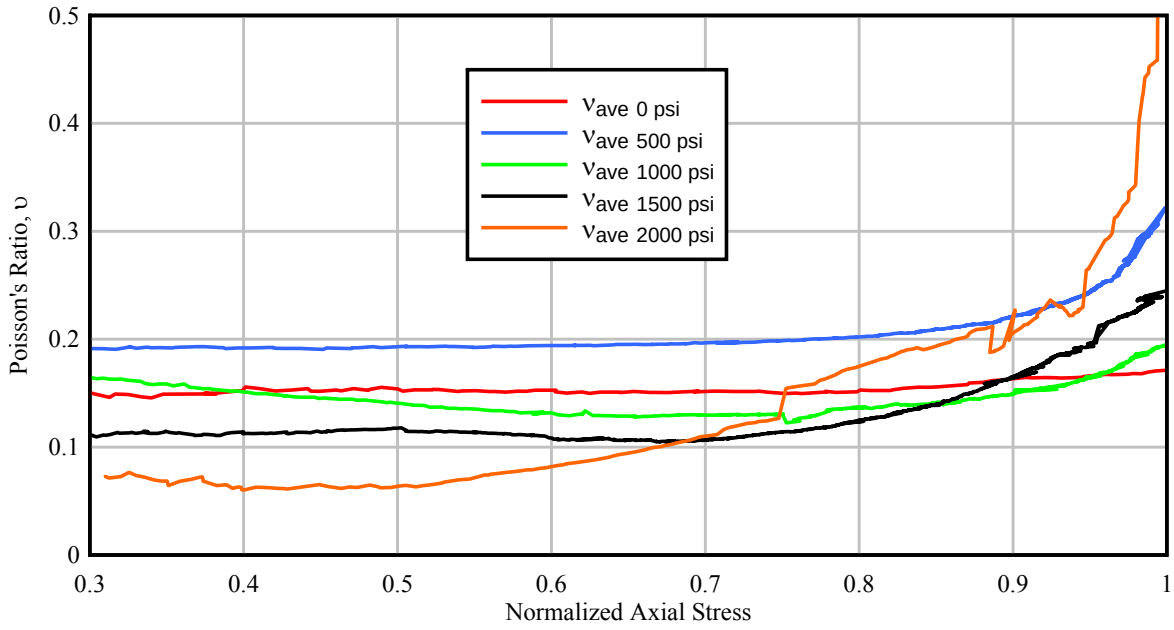


**Figure 5-3 Variation of instantaneous Poisson's ratio during application of axial load for all test series**

Gardner (1969) carried out triaxial compression tests on plain concrete specimens with an ultimate compressive strength of 4200 psi and confining pressures of 0, 1250, 2500, and 3750 psi. Fam (2000) used the results from Gardner (1969) to obtain a simplified expression that correlates the Poisson's ratio of the confined concrete as a function of level of confinement pressure. However, Fam (2000) excluded in his expression the triaxial

compression tests under a confining pressure of 2500 psi. The expression proposed by Fam (2000) is as follows:

$$\left(\frac{\nu_c}{\nu_{co}}\right) = C\left(\frac{\varepsilon_{cc}}{\varepsilon'_{cc}}\right) + 1 \qquad \text{[Eq. 1]}$$

Where:

- $\nu_c$ = Secant Poisson ratio
- $\nu_{co}$ = Initial Poisson ratio (i.e., initial slope of a plot of axial versus lateral strain)
- $\varepsilon_{cc}$ = Axial strain
- $\varepsilon'_{cc}$ = Axial strain at peak strain
- C = Constant obtained from linear regression using experimental data from Gardner (1969) which is shown in Figure 5-4

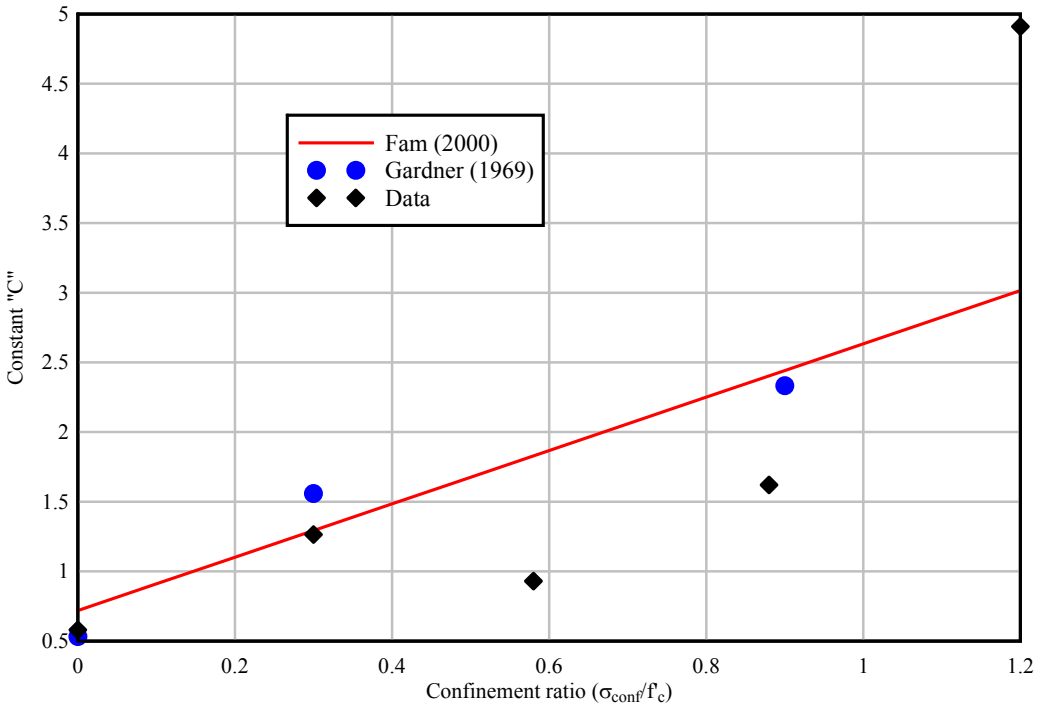


**Figure 5-4: Variation of constant "C" at different confinement ratios**

From Figure 5-4, it is evident that the expression proposed by Fam (2000) is accurate for low confinement ratios. As the confinement ratio increases, Fam's expression fails to capture the change in the value of constant "C" as determined through this experimental research.

Part of the objectives of this research was to investigate the stress-strain behavior of plain concrete specimens subjected to triaxial compression. In order to validate the stress-strain curves obtained in this research, a comparison of the axial stress – axial strain curves obtained experimentally versus those predicted by the Attard and Setunge (1996) model is presented in Figures 5-5 through 5-10.

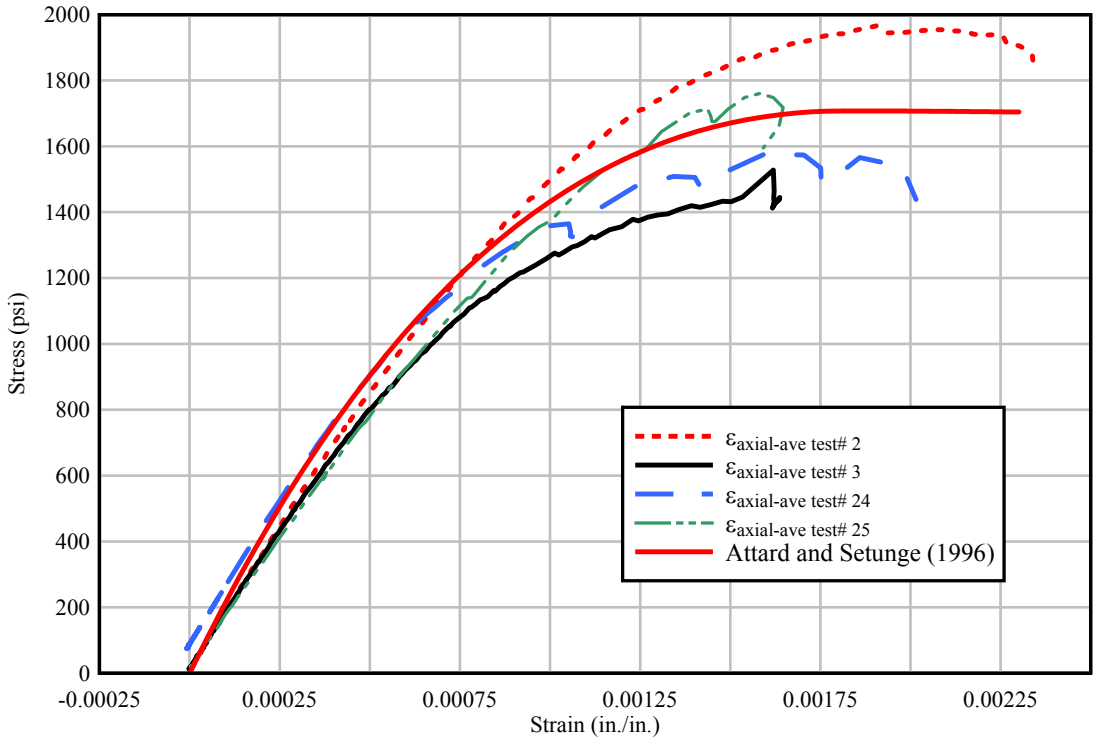


**Figure 5-5: Axial stress - axial strain curves from Unconfined Compressive tests**

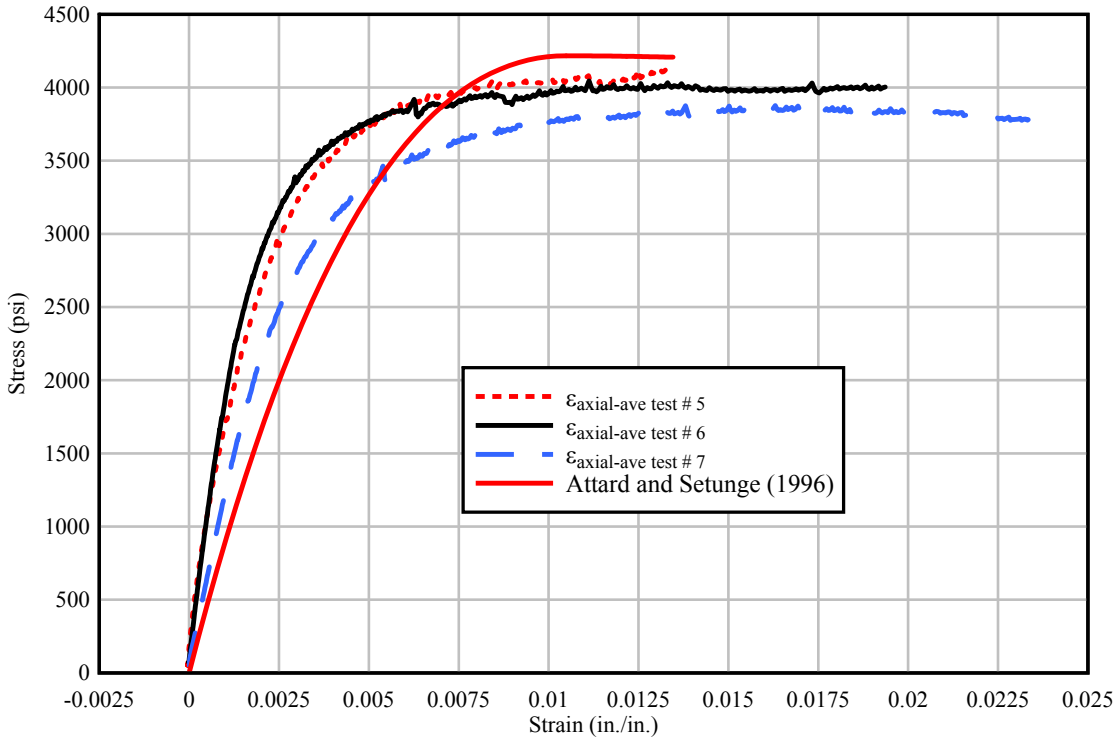


**Figure 5-6: Axial stress - axial strain curves from triaxial tests at a confining pressure of 500 psi**

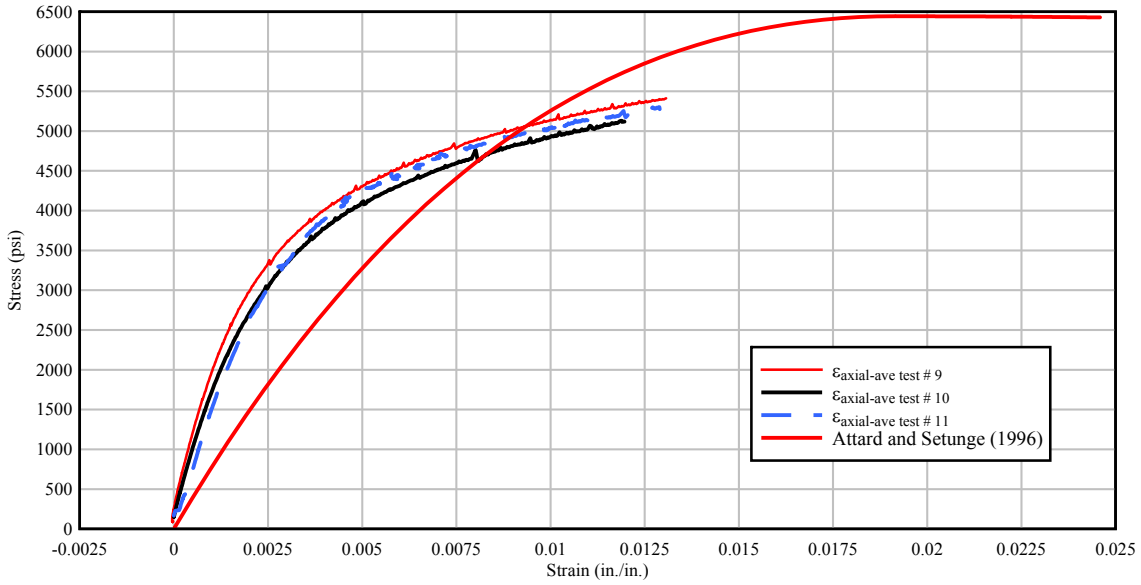


**Figure 5-7: Axial stress - axial strain from triaxial tests at a confining pressure of 1000 psi**

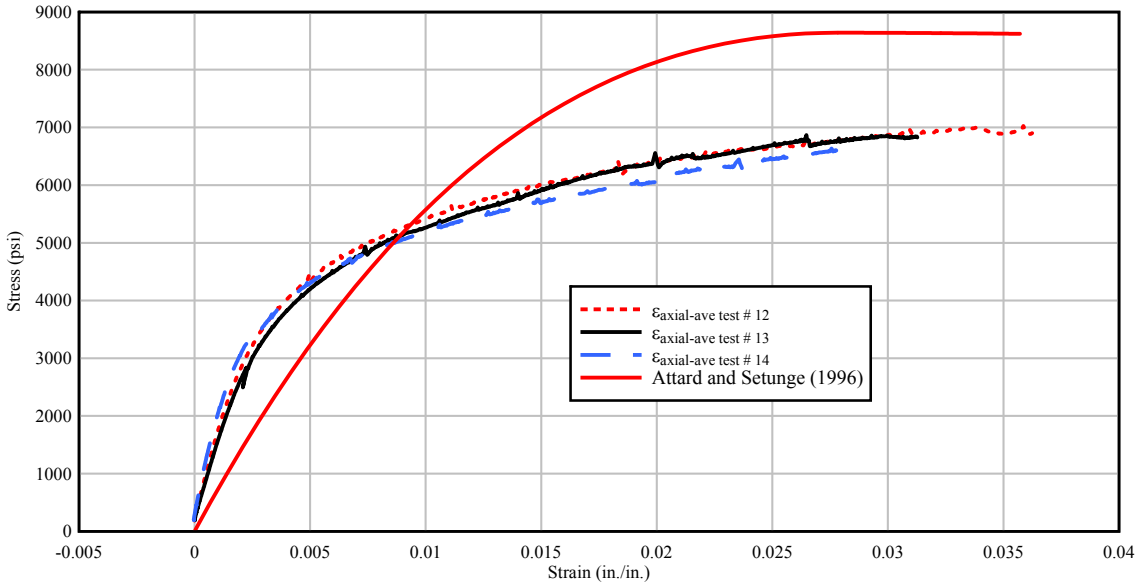


**Figure 5-8: Axial stress - axial strain from triaxial tests at a confining pressure of 1500 psi**

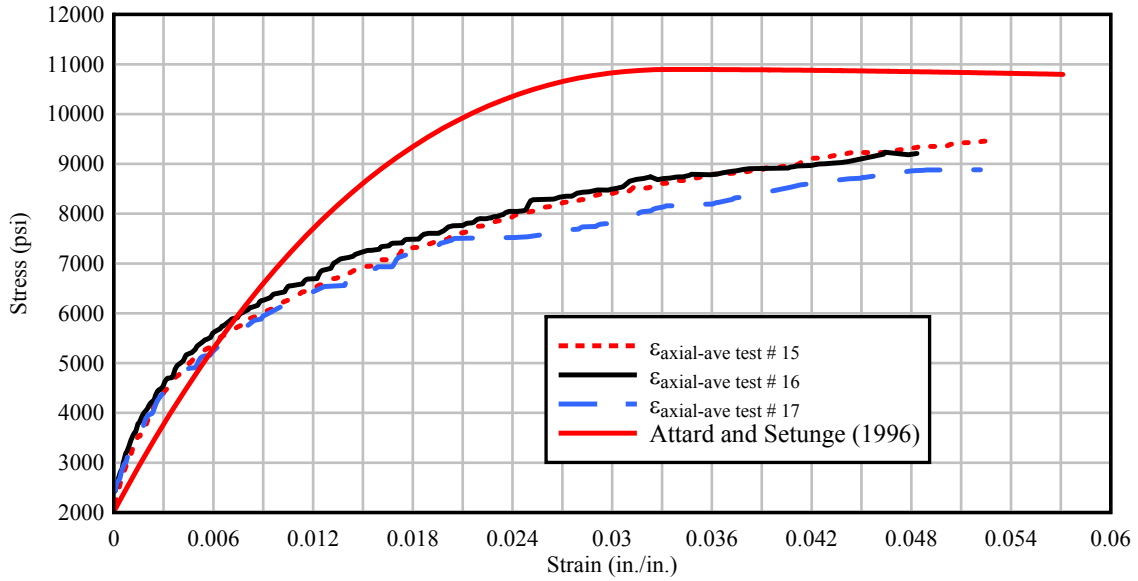


**Figure 5-9: Axial stress - axial strain from triaxial tests at a confining pressure of 2000 psi**

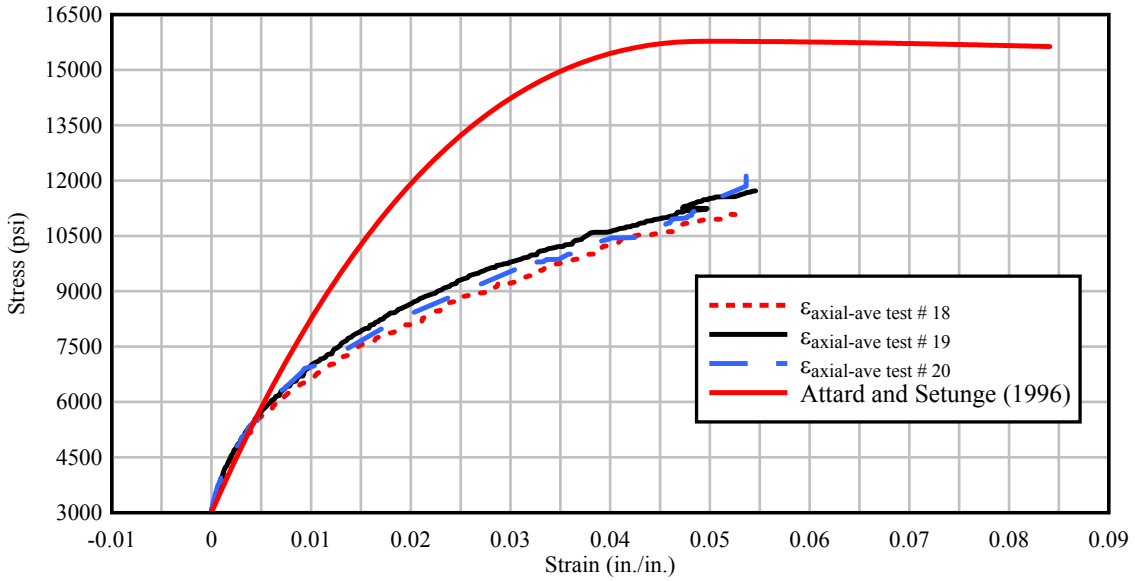


**Figure 5-10: Axial stress - axial strain from triaxial tests at a confining pressure of 3000 psi**

Figures 5-5 through 5-10 present a comparison between the experimental axial stress – axial strain curves obtained in this research to the curves predicted by the Attard and Setunge (1996) model. For the cases of no confinement and very limited confinement the experimental data and the model were in very good agreement. The model over-estimated axial stress at failure and failed to accurately capture the linear-elastic portion of the curves for the 1000 psi and 1500 psi test series. The initial portion of the curves were in better agreement for the 2000 psi and 3000 psi test series, although the model over-estimated axial stress at failure. In general, the comparison of the experimental curves versus the model, show that it predicts trends such as the general slope and the slope of the post-failure portion of the curves well but over-estimates stress and strain at failure.

# CHAPTER 6: CONCLUSIONS AND RECOMMENDATIONS

A summary of the results of this research project is presented herein. Some suggested changes to the experimental program used in this research are also mentioned. Finally, some recommendations for future work are mentioned.

Performance of the plain concrete specimens was evaluated from recorded stresses and strains during application of triaxial compression. Lateral confinement pressures were kept constant while axial compression was increased in a strain-controlled manner until failure.

The Mohr-Coulomb failure criterion was used to determine the angle of internal friction and apparent cohesion of the plain concrete studied.

Compressive strength of the plain concrete tested in this research increased as the lateral confinement provided during testing was increased. The results from the triaxial compression tests showed that the presence of lateral confinement added to the ultimate compressive strength of the specimen an amount approximately 3.5 times the lateral confinement pressure. An empirical failure envelope based on a linear correlation of the compressive strength experimental data obtained through this research was presented.

The experimentally determined full stress-strain curves have been presented from standard triaxial tests. At zero confinement, these curves exhibit a well-defined peak stress followed by a rapidly descending post-peak response. When confinement pressure was applied throughout these tests, the failure mechanisms transitioned from brittle to ductile failure modes, yielding a plateau post-peak response. These curves where used to determine other mechanical properties of the plain concrete such as Poisson's ratio, initial tangential

modulus, and provide empirical evidence of the effect that lateral confinement will have on these properties.

The value of the initial tangential modulus of the plain concrete studied tended to decrease as confinement pressures were increased, in other words, ductility of the plain concrete improved as confinement pressures applied to the specimens were increased. The progressive decrease in the initial slope of the stress-strain curves is in accordance with published data. The effect on ductility was also evidenced in the rise in magnitude of the ultimate axial and hoop strains due to increment in confining pressure applied.

The value of the instantaneous Poisson's ratio was determined for the plain concrete studied. Confining pressure had little effect on the ratio for values of the normalized axial stress below 0.8. At higher values, the effect on ductility if noticeable. Ductility, measured in terms of the instantaneous Poisson's ratio at failure, is greatly increased with increasing confinement pressures.

It is recommended that for future testing a hinged ring lateral deformeters and a linear potentiometer be used for radial and axial displacements, respectively. Triaxial tests should be conducted for 3000 psi and higher confinement pressures. The triaxial response of the plain concrete specimens should be modeled using a finite element modeling software and the results compared to the experimental data presented in this research and to data previously published to calibrate and validate the model.

# REFERENCES


Ahmad, S. H., and Shah, S. P. (1982). Complete Triaxial Stress-Strain Curves for Concrete, Journal of the Structural Division, ASCE, Vol. 108, No. ST4, Paper 17012, pp. 728-742.

Ahmad, S. H., Shah, S. P., and Khaloo, A. R. (1986). Orthotropic Model of Concrete for Triaxial Stresses, Journal of Structural Engineering, ASCE, Vol. 112, No. 1, Paper 20290, pp. 165-181.

Attard, M. M., and Setunge, S. (1996). Stress-Strain Relationship of Confined and Unconfined Concrete, ACI Materials Journal, Title no. 93-M49, pp. 1-11.

Binici, B. (2005). An analytical model for stress-strain behavior of confined concrete, Engineering Structures, Vol. 27, pp. 1040-1051.

Cedolin, L., Crutzen, Y. R. J., and Dei Poli, S. (1977). Triaxial Stress-Strain Relationship for Concrete, Journal of the Engineering Mechanics Division, ASCE, Vol. 103, No. EM3, Proc. Paper 12969, pp. 423-439.

Considere, A. (1906). Experimental Researches on Reinforced Concrete, Translation and Introduction by Leon L. Moisseiff, McGraw-Hill Book Co., Inc., New York, 2nd Edition.

Dahl, K. K. B. (1992). A Failure Criterion for Normal and High Strength Concrete. Rep. R. 286, Department of Structural Engineering, Technical University of Denmark, Lyngby, Denmark.

Dávila, J. F. (2007). Comportamiento Mecánico de Tubos de Material Compuesto Rellenos de Hormigón bajo Carga Axial en Compresión. M.S. thesis. University of Puerto Rico, Mayagüez, Puerto Rico, 226 pp.

Fam, A. Z. (2000). Concrete-filled Fiber Reinforced Tubes for Axial and Flexural Structural Members. PhD Thesis, the University of Manitoba, Canada, 261 pp.

Gardner, N. (1969). Triaxial Behavior of Concrete, Proceedings, American Concrete Institute, Vol. 66, No. 2, pp. 136-146.

Gerstle, Kurt H. (1981). Simple Formulation of Triaxial Concrete Behavior, ACI Journal, Proceedings, V. 78 No. 1, pp. 382-387.

Ghazi, M., Attard, M. M., and Foster, S. J. (2002). Modeling Triaxial Compression using the Microplane Formulation for Low Confinement, Computers and Structures, 80, pp. 919-934.

Hobbs, D. W. (1971). Strength of Concrete under Combined Stresses, Cement and Concrete Research, Vol. 1, pp. 41-56.

Hoek, E., and Franklin, J. A. (1968). A Simple Triaxial Cell for Field and Laboratory Testing of Rock, Trans. Instn Min. Metall., 77, A22-26.

Imran, I., and Pantazopoulou, S. (1996). Experimental Study of Plain Concrete under Triaxial Stress, ACI Material Journal, Vol. 93, No. 6, Nov-Dec 1996, pp. 589-601.

Imran, I., and Pantazopoulou, S. (2001). Plasticity Model for Concrete under Triaxial Compression, Journal of the Engineering Mechanics, ASCE, Vol. 127, No. 3, Paper 22206, pp. 281-290.

Issa, S. A., Islam, M. S., Issa, M. A., Yousif, A. A., and Issa, M. A. (2000). Specimen and Aggregate Size Effect on Concrete Compressive Strength, Cement, Concrete, and Aggregates, CCAGDP. Vol. 22, No. 2, pp. 103-115.

Mamlouk, M. S., and Zaniewski, J. P. (1999). Materials for Civil and Construction Engineers. Addison Wesley Longman, Inc., California, 388 pp.

Montoya, E., Vecchio, F. J., and Sheikh,S. A. (2006). Compression Field Modeling of Confined Concrete: Constitutive Models, Journal of Materials in Civil Engineering, ASCE, Vol. 18, No 4, pp. 510-517.

Oh, B., and Sause, R. (2006). Empirical Models for Confined Concrete under Uniaxial Loading, International Symposium on Confined Concrete, SP-238-9, pp. 141-156.

Palaniswamy, R. G., and Shah, S. P. (1975). A Model for Concrete Subjected to Triaxial Stresses, Cement and Concrete Research, Vol. 5, pp. 273-284.

Papanikolaou, V. K., and Kappos, A. J. (2007). Confinement-sensitive Plasticity Constitutive Model for Concrete in Triaxial Compression, International Journal of Solids and Structures, doi:10.1016/j.ijsolstr.2007.03.022.

Richart, F. E., Brandtzaeg, A., and Brown, R. L. (1928). A Study of the Failure of Concrete under Combined Compressive Stresses, Bulletin No. 185, Engineering Experiment Station, University of Illinois.

Rutland, C. A., and Wang, M. L. (1997). The Effects of Confinement on the Failure Orientation in Cementitious Materials, Experimental Observations, Cement and Concrete Composites, 19, pp. 149-160.

Sfer, D., Carol, I., Gettu, R., and Etse, G. (2002). Study of the Behavior of Concrete under Triaxial Compression, Journal of the Engineering Mechanics, ASCE, Vol. 128, No. 2, pp. 156-163.

Tan, T. H., and Sun, X. (2006). Failure Criteria of Concrete under Triaxial Compression, International Symposium on Confined Concrete, SP-238-15, pp. 235-247.

# APPENDIX A – EXPERIMENTAL TEST RESULTS

# APPENDIX A – EXPERIMENTAL TEST RESULTS

This appendix presents a summary of all the experimental data compiled for this ME research project. The following pages present the results of all the triaxial compression tests listed in the following table.

**Table A-1: Summary of Triaxial compression tests**

| Confining Stress, $\sigma_3$ (psi) | Number of Triaxial Compression Tests |
|---|---|
| 0 (unconfined) | 4 |
| 500 | 3 |
| 1000 | 3 |
| 1500 | 3 |
| 2000 | 3 |
| 3000 | 3 |
| 4000 | 1 |
| Total number of tests | 20 |

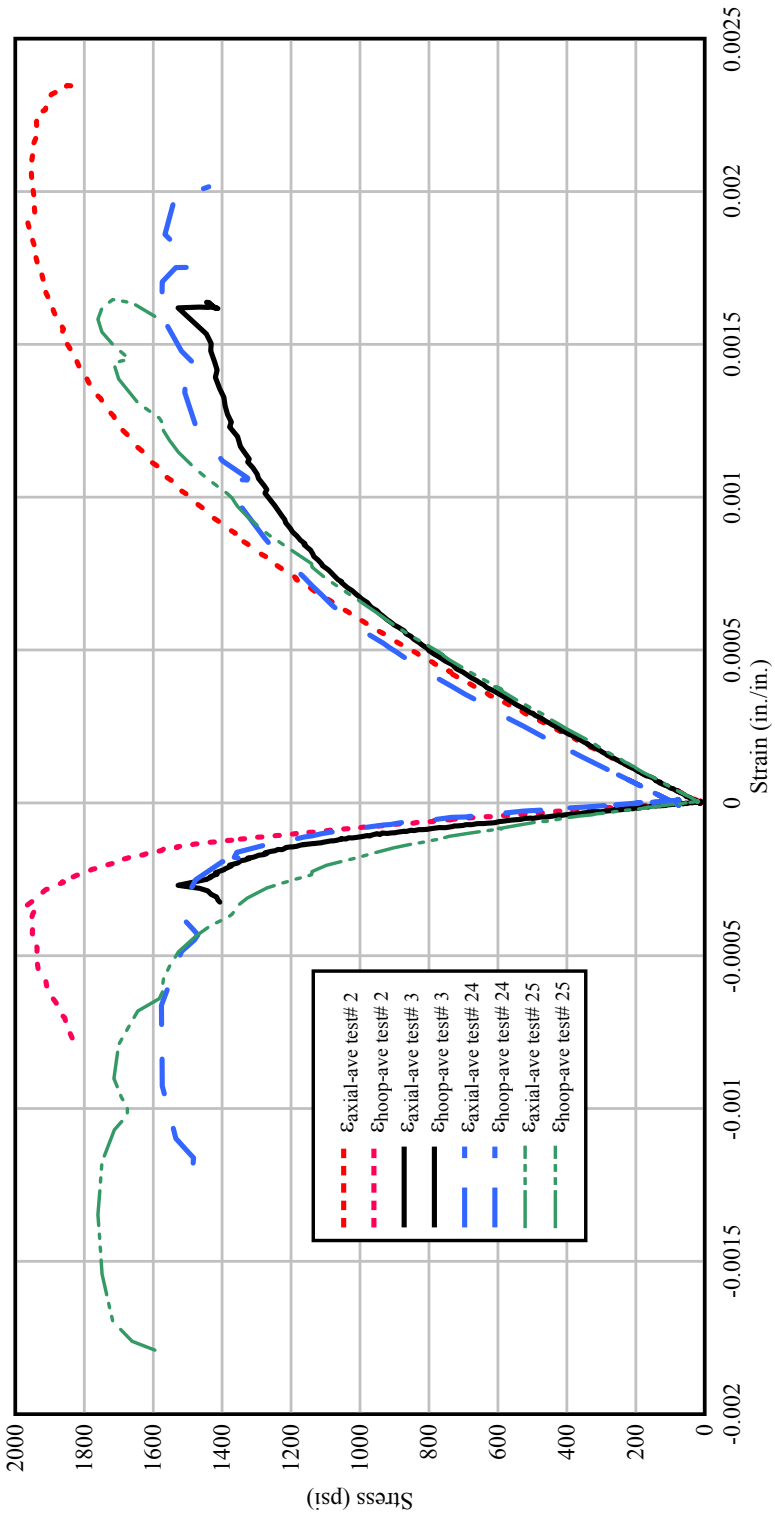


**Figure A-1: Stress-strain curves from Unconfined Compressive tests**

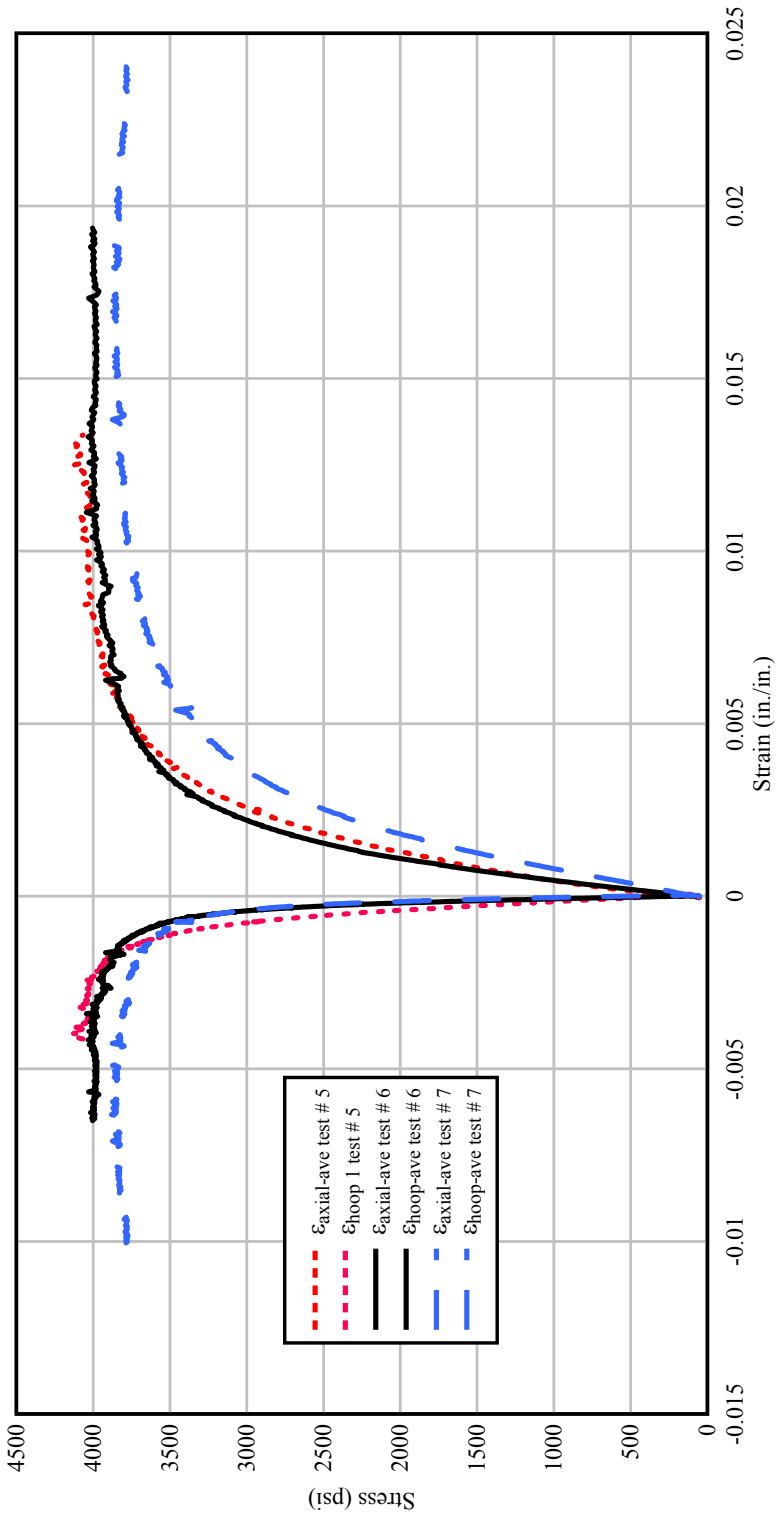


**Figure A-2: Stress-strain curves from triaxial tests at a confining pressure of 500 psi**

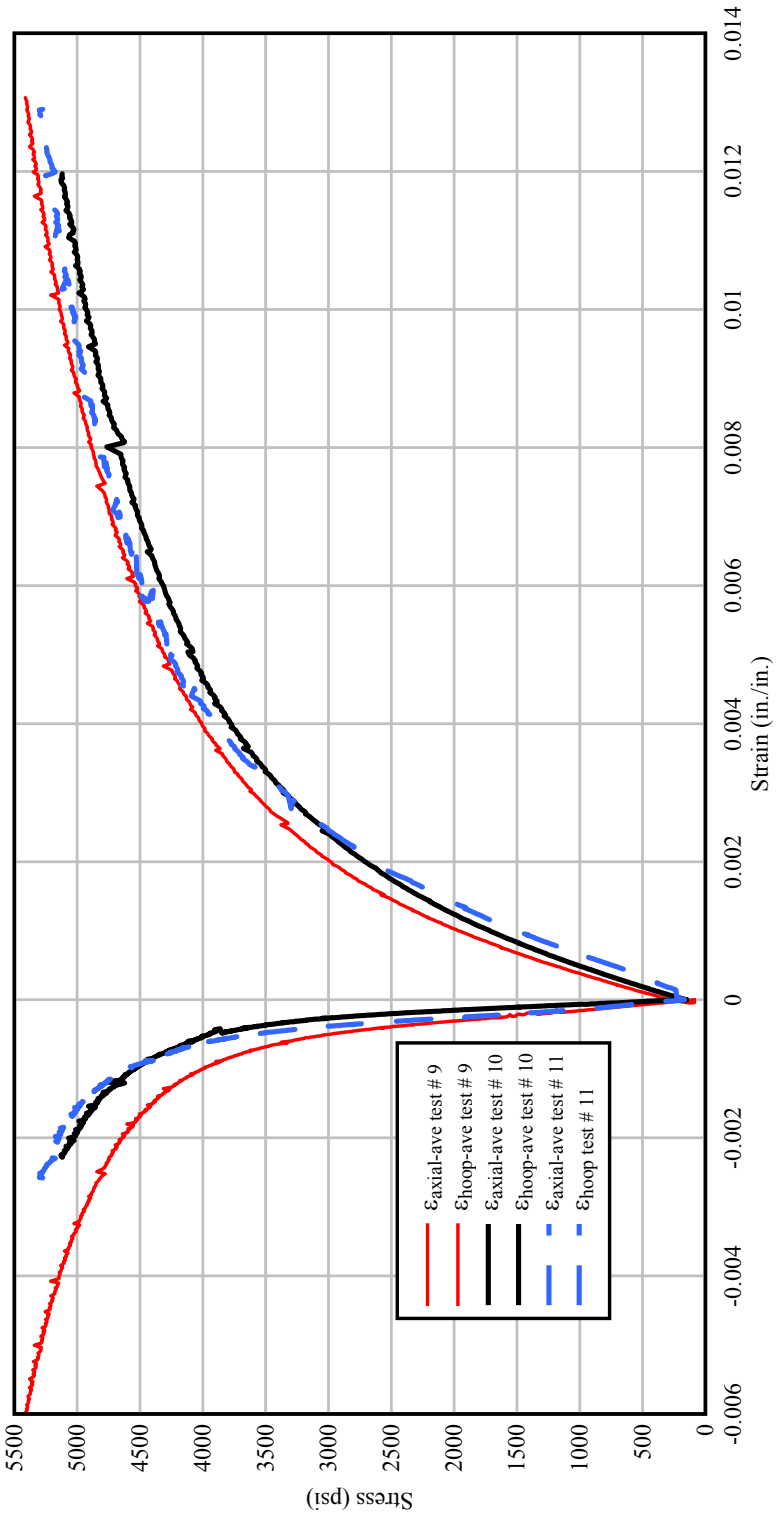


**Figure A-3: Stress-strain curves from triaxial tests at a confining pressure of 1000 psi**

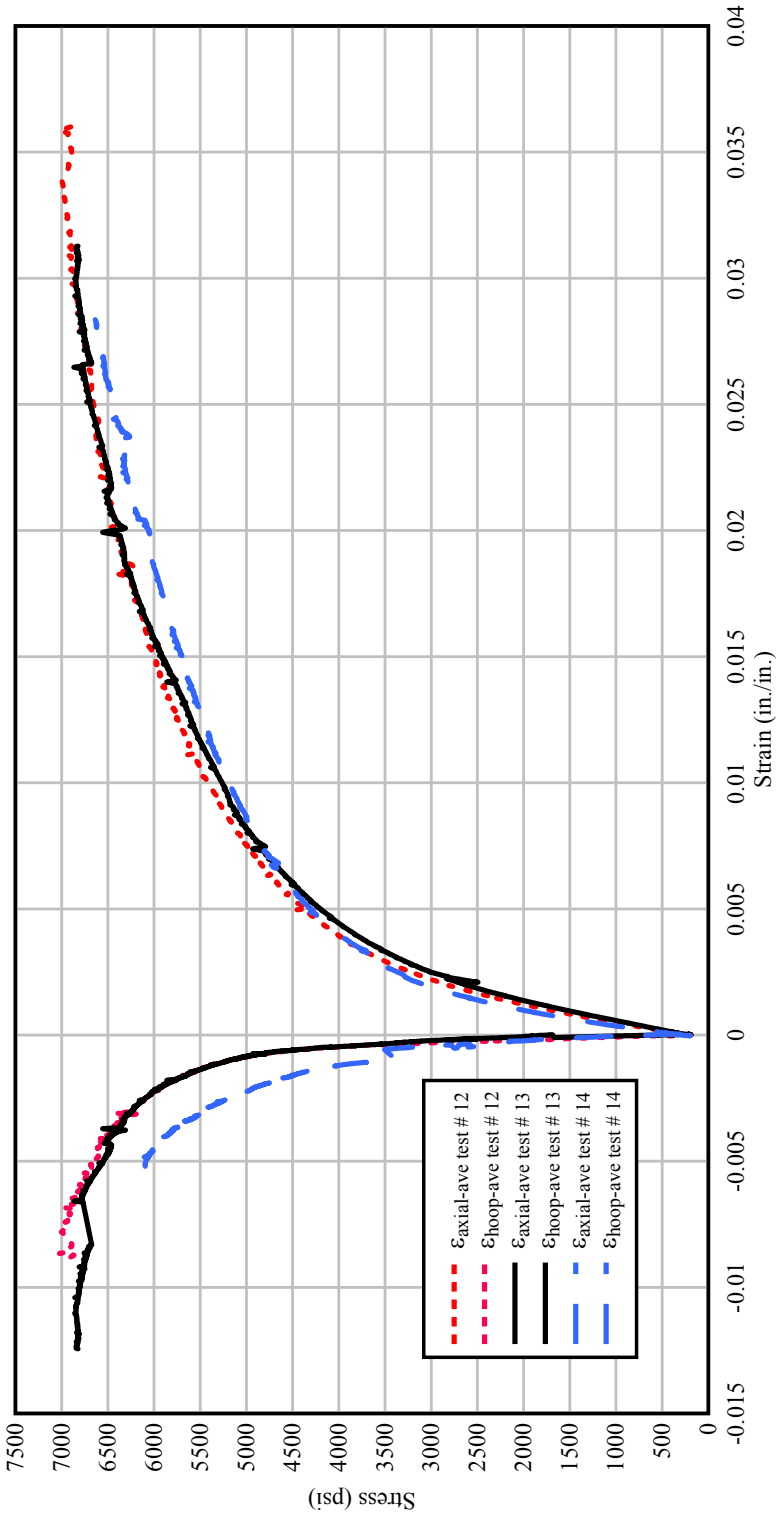


**Figure A-4: Stress-strain curves from triaxial tests at a confining pressure of 1500 psi**

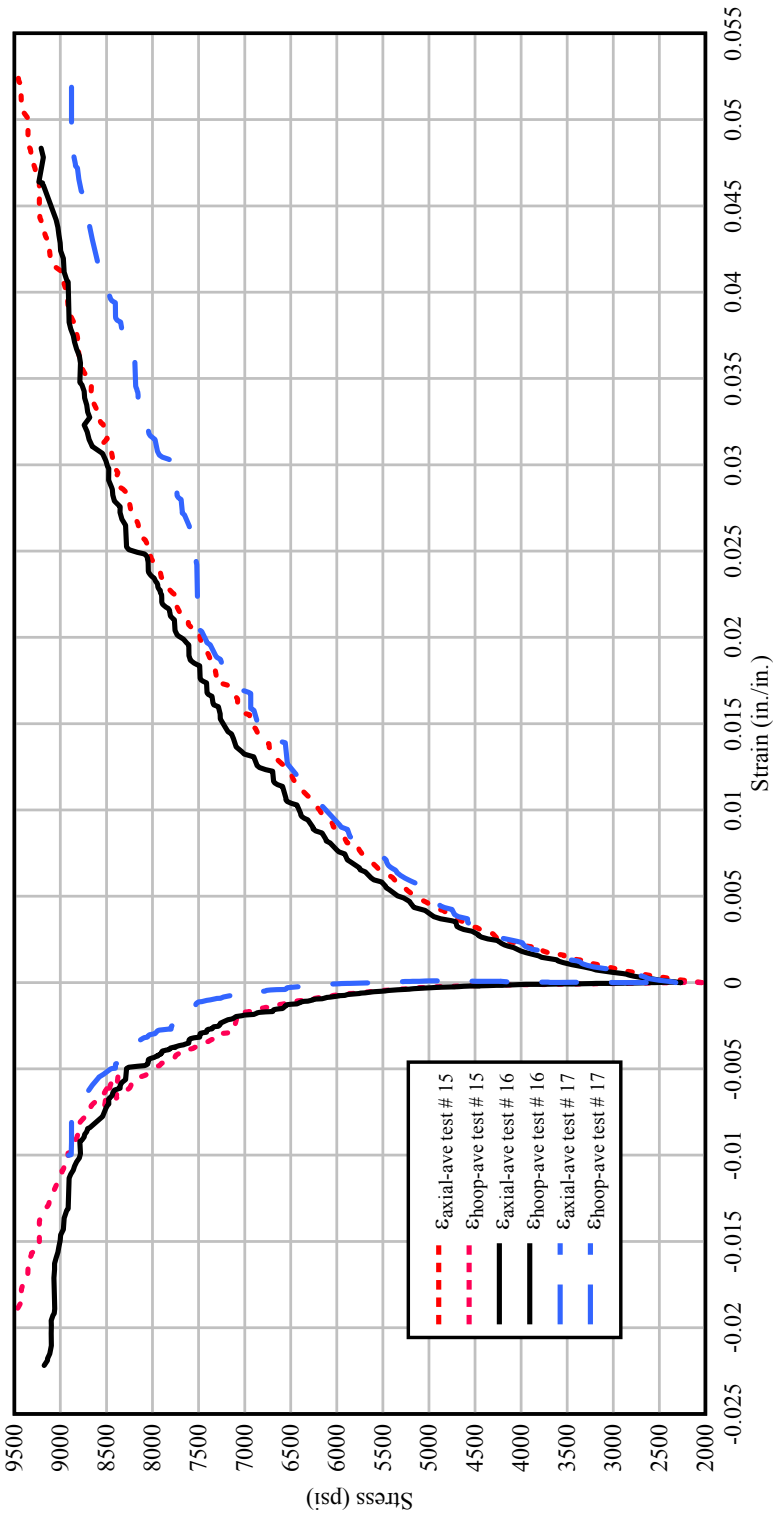


**Figure A-5: Stress-strain curves from triaxial tests at a confining pressure of 2000 psi**

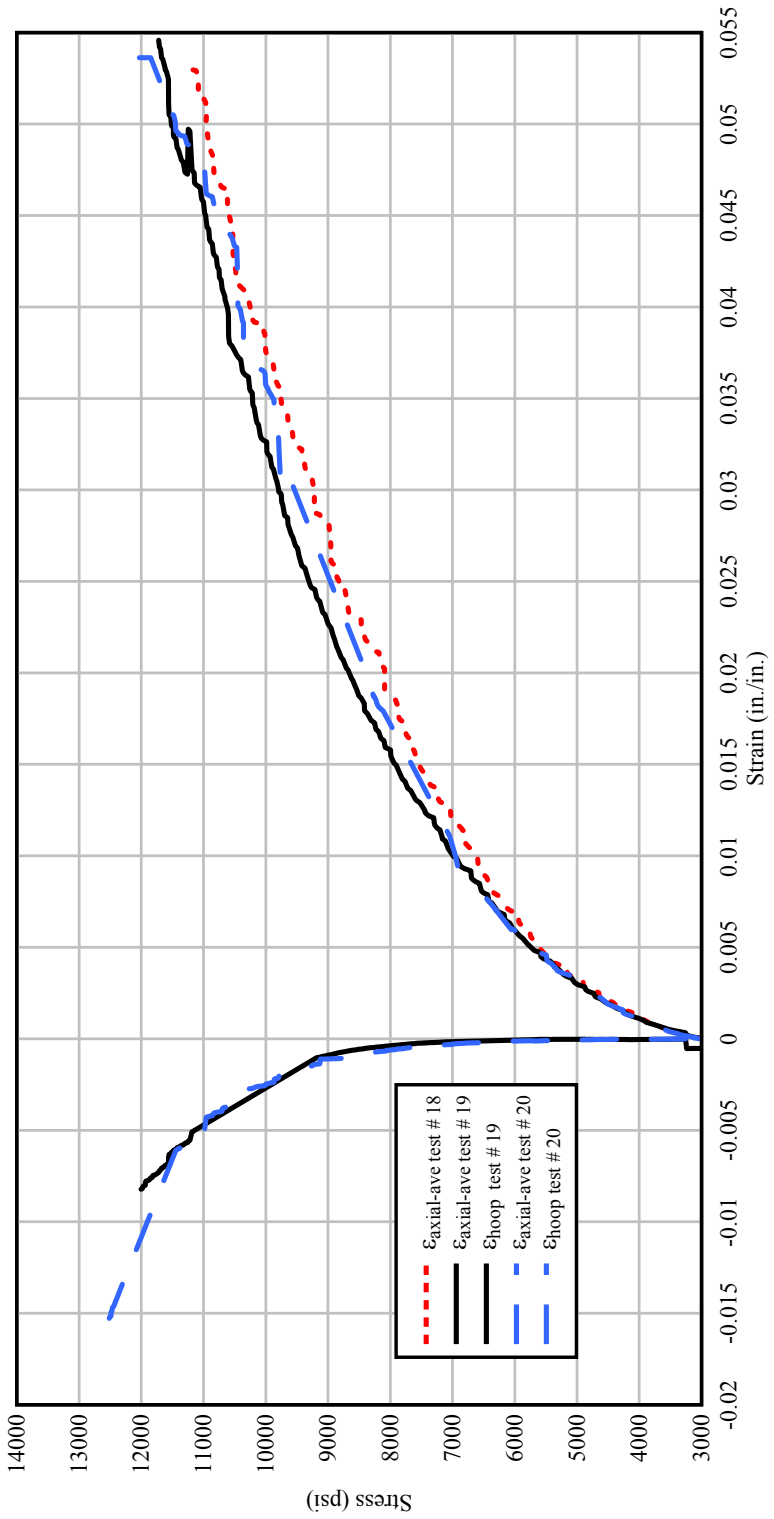


**Figure A-6: Stress-strain curves from triaxial tests at a confining pressure of 3000 psi**